

A Mutual Information-based Metric for Temporal Expressivity and Trainability Estimation in Quantum Policy Gradient Pipelines

Jaehun Jeong ,^{1,2,*} Donghwa Ji ,^{1,2,†} Junghee Ryu ,^{3,‡} and Kabgyun Jeong ,^{4,5,2,§}

¹*College of Liberal Studies, Seoul National University, Seoul 08826, South Korea*

²*Team QST, Seoul 08826, South Korea*

³*Division of National Supercomputing, Korea Institute of Science and Technology Information, Daejeon 34141, Republic of Korea*

⁴*Research Institute of Mathematics, Seoul National University, Seoul 08826, Korea*

⁵*School of Computational Sciences, Korea Institute for Advanced Study, Seoul 02455, Korea*

(Dated: December 8, 2025)

In recent years, various limitations of conventional supervised learning have been highlighted, leading to the emergence of reinforcement learning—and, further, quantum reinforcement learning that exploits quantum resources such as entanglement and superposition—as promising alternatives. Among the various reinforcement learning methodologies, gradient-based approaches, particularly policy gradient methods, are considered to have many benefits. Moreover, in the quantum regime, they also have a profit in that they can be readily implemented through parameterized quantum circuits (PQCs). From the perspective of learning, two indicators can be regarded as most crucial: expressivity and, for gradient-based methods, trainability. While a number of attempts have been made to quantify the expressivity and trainability of PQCs, clear efforts in the context of reinforcement learning have so far been lacking. Therefore, in this study, we newly define the notion of expressivity suited to reinforcement learning and demonstrate that the mutual information between action distribution and reward-signal distribution can, in certain respects, indicate information about both expressivity and trainability. Such research is valuable in that it provides an easy criterion for choosing among various PQCs employed in reinforcement learning, and further, enables the indirect estimation of learning progress even in black-box settings where the agent’s achievement aligned with the episodes cannot be explicitly evaluated.

I. INTRODUCTION

When one thinks of machine learning, the most immediate that comes to mind would be supervised learning, in which explicit answer labels are provided for each data sample and the model extracts some correlations between those input data and output labels so that it can infer the appropriate label even for new, unseen data. Supervised learning is typically categorized into two main tasks: regression and classification. Regression, in its simplest form exemplified by linear regression, can be understood as the problem of fitting a linear function that approximates well the given data-label distribution. Classification, on the other hand, deals with the task of determining to which of the pre-specified classes a new data sample belongs, often in a binary setup. These supervised learning frameworks have been studied extensively across various domains, especially with the advent of deep learning in the 2010s, which has achieved remarkable success in areas such as image classification and subfields of natural language processing.

Yet, supervised learning exhibits several limitations. Chief among these is that, when attempting to train machines to handle the diverse range of problems existing in the real world, it becomes impractical to provide explicit labels for every possible problem. For instance, consider the case of training a four-legged robot that must learn to walk [1]. Given the wide variety of physical environments it may encounter—such as

stairs, inclined surface of varying slopes, or public transportation systems like buses and subways—it would be almost impossible to prescribe explicit labels in advance such as “adjust this component of the body in this precise way” for every scenario, especially when the infinity of possible real-world conditions is taken into account. Even if possible, such an approach would be highly inefficient. This challenge of providing explicit labels extends beyond just robotics and is a recurring issue across many problem domains.

In this respect, reinforcement learning (RL) has been regarded as a major paradigm to overcome this shortcomings of supervised learning. Instead of requiring deterministic answer labels, RL provides the agent with a reward that reflects how close its chosen action is to an ideal one within a given specific learning environment, and the agent learns accordingly. Among the various pipelines developed under this framework, policy gradient methods, which update policy functions through gradient ascent to approach an optimal policy, stand out. This method is particularly attractive since it allows learning even with only limited information about the environment, and as it is one of the gradient-based methods, it can benefit from the power of existing well-devised optimizers—such as Adam.

More recently, with the growing interest in the potential advantages of quantum computing over classical computing, there has been a surge of research attempting to bring reinforcement learning into quantum computational settings. Policy gradient methods are no exception, as they can be easily understood as one type of variational quantum algorithms similar to the Variational Quantum Eigensolver (VQE). Accordingly, one can relatively readily and intuitively implement such algorithms by designing suitable parameterized quantum circuits (PQCs). While numerous proposals have explored

* abin1125@snu.ac.kr

† donghwa722@gmail.com

‡ junghee@kisti.re.kr

§ kjeong6@snu.ac.kr

different designs, in this study we employ the reuploading-based parameterized quantum circuit proposed by *Jerbi et al.* [2], which is currently considered one of the most effective designs in terms of overall performance.

From the perspective of learning theory, whether classical or quantum, two indicators are widely recognized as critical: expressivity and trainability. Expressivity, which measures how well a model—or in the quantum case, a PQC—can represent or approximate a wide range of functions, is important as it is related closely to the fundamental bias-variance tradeoff. Trainability, on the other hand, concerns how well gradient-based methods avoid issues such as vanishing gradients (e.g. Barren Plateau) or divergence, and how reliably they converge toward optimal solutions. Since this fundamentally governs the likelihood and stability of successful learning, there is a clear need for suitable quantitative measures of trainability.

Although many efforts have been devoted to quantifying these two indicators—either independently [3, 4] or jointly [5]—they have exhibited limitations. In particular, they both are not suitable to capture the dynamic, time-varying nature of expressivity that arises from the exploitation-exploration tradeoff, which is central to reinforcement learning. Moreover, many approaches rely on quantifying those indicators only at initialization, for randomly selected parameter values, thereby reflecting merely the potential coverage of functions or overall learning stability, thus not appropriate to account for the inherently dynamic nature of the reinforcement learning paradigm.

To address these issues, in this work we propose a new definition of expressivity tailored to reinforcement learning and introduce mutual information between the action distribution and the reward-signal distribution as an indirect measure that can effectively track both that expressivity and trainability over episodes, in the context of the quantum policy gradient methods. More concretely, we formalize the relationship between the gradient norm and mutual information, as well as between our newly defined expressivity notion and mutual information, in the form of inequalities. Through this analysis, we demonstrate that mutual information serves as a useful and efficient indicator capable of monitoring both expressivity and trainability in quantum reinforcement learning settings.

II. PRELIMINARY

A. Policy Gradient Fundamentals

First we give a slight introduction to reinforcement learning and policy gradient statements for those who find these concepts unfamiliar. Note that these are the slight modifications from the introductory notes [1].

To describe many reinforcement learning environments in a formal mathematical way, **Markov Decision Process (MDP)** is commonly used.

Definition 1 (Markov Decision Process). *Any reinforcement learning environments can be simplified to just a tuple of $(S, A, \{P_{sa}\}, \gamma, R, \pi)$, which is given as follows:*

- S : set of states, A : set of actions, $\{P_{sa}\}$: state transition probabilities.

- The environment shows the agent a certain state, and the agent interacts with the environment by selecting the optimal action according to that. After this one-shot game, the environment changes the state stochastically depending on the prefixed probability P_{sa} .

- γ : discount factor, $\gamma \in [0, 1)$.
 - It is given just for the case where the expected total payoff diverges.
- R : reward function, $S \times A \rightarrow \mathbb{R}$.
 - It works as a baseline referred by the agent when updating its own policy.
- π : policy function, $S \rightarrow P_{SA}$.
 - It gets input of a current state, and outputs the probability distribution of the actions with that fixed state.

With this mathematical framework, the primary objective in this reinforcement learning regime becomes maximizing the **expected total payoff**, which is

$$\mathbb{E} [R(s_0, a_0) + \gamma R(s_1, a_1) + \gamma^2 R(s_2, a_2) + \dots]$$

and can be seen as our objective function, by fine-tuning the policy function π . Next question is now then, *how we maximize this objective function?*

There are many algorithms to do this job, such as well-known value function iteration and policy iteration, but in this work, as mentioned earlier, we will focus on a gradient-based one, **policy gradient**. To reach further to the policy gradient, there are some assumptions that are required to be satisfied.

- We only consider the case with finite horizon T , which signifies the game definitely, in a finite timestamp, ends.
- Our policy function is actually a randomized policy π_θ with parameterized by trainable θ ; hence the policy function is also trainable.

Moreover, we introduce some useful definitions and notations here:

- Trajectory τ : $(s_0, a_0, \dots, s_{T-1}, a_{T-1}, s_T)$
 - It can be viewed as *learning history*, basically.
- We will notate the distribution of the trajectories τ as $P_\theta(\tau)$.
- Let us notate the total payoff with the fixed, specific τ as $f(\tau) = \sum_{t=0}^{T-1} \gamma^t R(s_t, a_t)$.

Now we can rephrase our objective function defined earlier as

$$\eta(\theta) := \mathbb{E}_{\tau \sim P_\theta} [f(\tau)] = \int P_\theta(\tau) f(\tau) d\tau \quad (1)$$

and apply the gradient ascent method to this and update θ accordingly. One observation is that

$$\nabla \eta(\theta) = \int (\nabla P_\theta(\tau)) f(\tau) d\tau \quad (2)$$

$$= \int (\nabla \log P_\theta(\tau) P_\theta(\tau)) f(\tau) d\tau \quad (3)$$

$$= \mathbb{E} [(\nabla \log P_\theta(\tau)) f(\tau)]. \quad (4)$$

Next step is to calculate $\nabla \log P_\theta(\tau)$. Note that

$$P_\theta(\tau) = \mu(s_0) \pi_\theta(a_0|s_0) P_{s_0 a_0}(s_1) \cdots P_{s_{T-1} a_{T-1}}(s_T), \quad (5)$$

where μ is an one distribution of states that gives us the probability of a certain state being chosen for the initial state. Then we can consider the log-derivatives,

$$\begin{aligned} \log P_\theta(\tau) &= \log \mu(s_0) + \log \pi_\theta(a_0|s_0) \\ &\quad + \sum_{i=0}^{T-1} \log P_{s_i a_i}(s_{i+1}), \end{aligned} \quad (6)$$

$$\nabla \log P_\theta(\tau) = \sum_{t=0}^{T-1} \nabla \log \pi_\theta(a_t|s_t). \quad (7)$$

One interesting fact here is that we don't need to know of μ and P_{sa} in advance; that is one of the reasons why this policy gradient is favored when the information of the environment is limited, which is a common situation.

Substituting the equation (6) into (3), we get

$$\nabla \eta(\theta) = \mathbb{E} \left[\left(\sum_{t=0}^{T-1} \nabla \log \pi_\theta(a_t|s_t) \right) \left(\sum_{t=0}^{T-1} \gamma^t R(s_t, a_t) \right) \right]. \quad (8)$$

Moreover, we can easily prove that

$$\mathbb{E} \left[\nabla \log \pi_\theta(a_t|s_t) \cdot \sum_{j < t} \gamma^j R(s_j, a_j) \right] = 0 \quad (9)$$

and the above equation (7) now simplifies to

$$\nabla \eta(\theta) = \mathbb{E} \left[\sum_{t=0}^{T-1} \left(\nabla \log \pi_\theta(a_t|s_t) \cdot \left(\sum_{j=t}^{T-1} \gamma^j R(s_j, a_j) \right) \right) \right]. \quad (10)$$

Let us introduce some new notations,

$$G_t := \sum_{j=t}^{T-1} \gamma^j R_j. \quad (11)$$

Then,

$$\mathbb{E} [\nabla \log \pi_\theta(a_t|s_t) \cdot G_t]$$

$$= \mathbb{E} [\mathbb{E} [\nabla \log \pi_\theta(a_t|s_t) \cdot G_t|s_t, a_t]] \quad (12)$$

$$= \mathbb{E} [\nabla \log \pi_\theta(a_t|s_t) \cdot \mathbb{E} [G_t|s_t, a_t]]. \quad (13)$$

Now we see the form of the conventional Q function, that is,

$$Q^\pi(s, a) := \mathbb{E} \left[\sum_{k=0}^{T-t-1} \gamma^{t+k} R_{t+k} \middle| s_t = s, a_t = a \right]. \quad (14)$$

Thus, it again gets rephrased as

$$\mathbb{E} [\nabla \log \pi_\theta(a_t|s_t) \cdot G_t] = \mathbb{E} [\nabla \log \pi_\theta(a_t|s_t) \cdot Q^{\pi_\theta}(s_t, a_t)]. \quad (15)$$

Now,

$$\nabla \eta(\theta) = \mathbb{E} \left[\sum_{t=0}^{T-1} \nabla \log \pi_\theta(a_t|s_t) \cdot G_t \right] \quad (16)$$

$$= \sum_{t=0}^{T-1} \mathbb{E} [\nabla \log \pi_\theta(a_t|s_t) \cdot G_t] \quad (17)$$

$$= \sum_{t=0}^{T-1} \mathbb{E} [\nabla \log \pi_\theta(a_t|s_t) \cdot Q^{\pi_\theta}(s_t, a_t)]. \quad (18)$$

Consequently, the choice between G_t and Q^{π_θ} for gradient estimation is interchangeable, and we will use the notation $Y \in \{G_t, Q^{\pi_\theta}\}$ from now on this work.

B. Quantum Policy Gradient Framework

Basically, to port classical reinforcement learning to its quantum counterpart, one widely used pipeline during these days of noisy intermediate-scale quantum (NISQ) era is of the hybrid quantum machine learning approach, where certain hypothesis family for a given learning task is realized by parameterized and data-dependent quantum computations while a classical optimization algorithm is used to train them. More practically, those quantum parts are generally given as parameterized quantum circuits (PQCs), which have been proved to solve various learning tasks efficiently.

In the paper [2], the authors discriminated two approaches, *raw-PQC* and *softmax-PQC*, claiming the latter is more suitable for the reinforcement learning structure since it reflects the inborn *greediness* by parameter β . The whole quantum circuit, which is shown in Fig. 1 of [2] is characterized by trainable parameters (ϕ, λ, ω) , which are rotation angles, scaling parameters, and the weight of the Hermitian measurement operators, respectively. Note that the state is not encoded at once, rather being reuploaded multiple times during the whole circuit evaluation, with the scaling parameters λ .

And the whole quantum policy gradient algorithm we adopted from the [2] is given as

Algorithm 1 REINFORCE with PQC policies and value-function baselines - from [2]

```

1: Input: a PQC policy  $\pi_\theta$ ; a value-function approximator  $\tilde{V}_\omega$ 
2: Initialize parameters  $\theta$  and  $\omega$ ;
3: while True do
4:   Generate  $N$  episodes  $\{(s_0, a_0, r_1, \dots, s_{H-1}, a_{H-1}, r_H)\}_i$ 
   following  $\pi_\theta$ 
5:   for episode  $i$  in batch do
6:     Compute the returns  $G_{i,t} \leftarrow \sum_{t'=1}^{H-t} \gamma^{t'} r_{t+t'}^{(i)}$ 
7:     Compute the gradients  $\nabla_\theta \log \pi_\theta(a_t^{(i)} | s_t^{(i)})$ 
8:     Fit  $\{\tilde{V}_\omega(s_t^{(i)})\}_{i,t}$  to the returns  $\{G_{i,t}\}_{i,t}$ ;
9:   end for
10:  Compute  $\Delta\theta \leftarrow \frac{1}{N} \sum_{i=1}^N \sum_{t=0}^{H-1} \nabla_\theta \log \pi_\theta(a_t^{(i)} | s_t^{(i)}) (G_{i,t} - \tilde{V}_\omega(s_t^{(i)}))$ ;
11:  Update  $\theta \leftarrow \theta + \alpha \Delta\theta$ ;
12: end while

```

which is quite similar to what have been introduced earlier in policy gradient statements, except for the part of the baseline. It is often used to reduce the variance of gradient estimation and as stated in Algorithm 1, the value-function approximator is one of the popular choices [1, 6, 7]. Yet, for the sake of simplicity, we will not use complex value function approximator-like baseline techniques. Instead, we employ a common variance reduction method by normalizing the collected returns (i.e., standardizing them by subtracting the batch mean and dividing by the batch standard deviation).

C. Concepts of Expressivity and Trainability

Whether classical or quantum setting, when we consider the somewhat ‘learning’ task especially with gradient-based methods, two concepts hold significant importance; expressivity and trainability. Particularly by following the approximation theory’s perspective, learning is defined statistically to be the task of finding the optimal approximation function \hat{f}_n within certain function class \mathcal{F} (e.g. neural networks) of the real, unknown function f_ρ (e.g. true regression function), based on the observed dataset $\mathcal{D} = \{(x_i, y_i)\}_{i=1}^n$ [8]. Thinking of the regression model

$$y_i = f_\rho(x_i) + \epsilon_i, \quad i = 1, 2, \dots, n. \quad (19)$$

Our ultimate goal is finding the minimizer of so called population risk $\mathcal{E}(f)$, which is defined as

$$\mathcal{E}(f) := \mathbb{E}_{(\mathbf{x}, \mathbf{y}) \sim \rho} [(\mathbf{y} - f(\mathbf{x}))^2], \quad (20)$$

where ρ denotes the joint distribution of \mathbf{x} and \mathbf{y} , as given. However, it is hardly known the true ρ in most of the cases, thus we rather consider the empirical risk minimizer \hat{f}_n on the dataset D ,

$$\hat{f}_n = \operatorname{argmin}_{f \in \mathcal{F}} \mathcal{E}_D(f) \quad (21)$$

$$:= \operatorname{argmin}_{f \in \mathcal{F}} \left[\frac{1}{n} \sum_{i=1}^n (y_i - f(x_i))^2 \right]. \quad (22)$$

Now the concept of excess risk is induced, which is $\mathbb{E}_{\mathbf{X} \sim \rho_X} [(\hat{f}_n(\mathbf{X}) - f_\rho(\mathbf{X}))^2]$. It serves as an important statistical metric directly measuring the generalizability of our candidate function \hat{f}_n in the unseen data setting. Interestingly, it is well known that the following inequality holds [9]:

$$\mathbb{E}_{\mathbf{X} \sim \rho_X} [(\hat{f}_n(\mathbf{X}) - f_\rho(\mathbf{X}))^2] \leq \frac{\text{Complexity Measure of } \mathcal{F}}{n} + \text{Approx. Error}^2 \quad (23)$$

The right-hand side can be seen as reflecting a trade-off between the approximation error and the complexity of the function class \mathcal{F} .

This concept is not limited to regression and can be extended to other learning tasks, where it is commonly recognized as the bias-variance tradeoff. This leads to two common issues. If the model’s complexity (i.e., the complexity of \mathcal{F}) is too low, the model is prone to underfitting. This state is characterized by high bias, resulting in poor generalization performance because the model fails to capture the underlying structure of the data. Conversely, if the model’s complexity is too high, the model is prone to overfitting. This occurs when the model performs exceptionally well on the training data but poorly on unseen test data. Such a model suffers from high variance; its excessive complexity has caused it to memorize noise and artifacts specific to the training set rather than learning the true, generalizable signal. Moreover, in contrast to classical models where test error typically follows a U-shaped curve (a single descent), modern over-parameterized deep learning models often exhibit the ‘double descent’ phenomenon. This phenomenon reveals that increasing model complexity far beyond the classical overfitting point can lead to a second descent in test error, often achieving performance superior to the original ‘sweet spot’ [10]. Thus, whether considering the classical machine learning model or the modern deep learning model, the task of measuring the given model’s complexity remains to be an important task [11, 12].

Actually, the term ‘expressivity’ is widely used without the clear distinction with ‘complexity’ and ‘capacity’, since they all share the same intuitive concept [13]. Yet, in the reinforcement learning regime, since its model outputs somewhat distribution and the deviation of those distributions through multiple evaluations becomes an important metric, we will use the term ‘expressivity’ during this paper, which we think literally natural to capture those fundamentals.

As mentioned earlier, since the parameterized quantum circuits take the role of function class \mathcal{F} theoretically, measuring the given circuit’s complexity properly also remains significant in the quantum machine learning paradigm. There have been one notable attempt to tackle this issue, shown in the [3]. In this study, the author measures expressivity by the deviation between the two, output state’s fidelity distribution between the target PQC and Haar random circuit. Even though these attempts might work well for the conventional supervised learning tasks, we conceived it is not suitable for reinforcement learning environments, since it just measures the ‘static’, ‘fixed’ models’ complexity through multiple times of sampling, while what is really important in RL is

the actual ‘temporal, time dependent fluctuation’ of the policy function’s expressivity considering the fundamentals of exploitation-exploration concept in RL [2]; this discussion will be further described in the main results section.

Meanwhile, when using some gradient-based method such as gradient descent/ascent, the issue of trainability also becomes one dominant problem. This informal concept of trainability, signifies literally *how well the optimization goal is achieved without any issues such as gradient vanishing/exploding, too much oscillation or even the divergence, which is actually the failure of given learning task*. There have been some papers considering these issues, for instance gradient vanishing or exploding in the classical deep learning models, since it also utilizes gradient information for updating the parameter [14]. With this trainability concept in mind, one can view the Adam optimizer [15], as the one of the most hopeful optimizers proposed to solve this trainability issue, as well.

In the quantum computation regime, one can easily observe the phenomena of ‘Barren Plateau’, which is a quantum counterpart of the gradient vanishing problem [16]. In that work, the authors examined the empirical results that random circuits might be an unsuitable choice for moderately many qubits circuit while also claiming that the gradient might be concentrated to zero, which is non-utilizable, with exponentially probability decay with the number of qubits. Thus, considering the number of qubits is a fundamental parameter defining the given quantum circuit’s complexity, one can easily find that the expressivity and trainability is correlated to the certain, significant extent; and that motivates us to develop one novel metric which can track both of them simultaneously.

A nice reference for this trainability notion is [4]. The authors utilize the fisher information matrix spectrum, which shows how the eigenvalues of the fisher information matrix are distributed. Intuitively, one can expect the optimization performance of the model which has more concentrated eigenvalues to the zero would be poor and vice versa, since the former might signify more ‘flat’ curvature of the loss landscape; and this is well discussed in the Figure 2 and 3 of that paper. Interestingly, this intuition holds true thus bridging the convergence speed and the fisher information spectrum in a trainability manner. However, this approach (or metric) for trainability is still not feasible for the reinforcement learning environment since it calculates ‘empirical’ fisher information matrix with ‘randomly’ sampled parameter sets and data sets at first glance, again based on the model’s static and fixed structure. What is rather important in reinforcement learning is how the gradient or its variance gets concentrated to zero during the whole learning episodes of the agent, which can be viewed to be more ‘temporal’; and that motivates us to introduce the concept of MI-TET, Mutual Information-based Temporal Expressivity and Trainability estimator.

III. MAIN RESULTS

A. Formulation of MI-TET

First of all, let us give the formal definition of **MI-TET**, *Mutual Information-based Temporal Expressivity and Trainability measure*.

Definition 2 (MI-TET, Mutual Information-based Temporal Expressivity and Trainability). *Let $Y \in \{G_t, Q^{\pi_\theta}\}$ and assume $Y_{\min} \leq Y \leq Y_{\max}$. Based on the prefixed parameter B (Bin count), fix the interval parameter $\delta > 0$ and divide $[Y_{\min}, Y_{\max}]$ into non-overlapping sections*

$$B_k := [b_k, b_k + \delta), \quad k \in \{1, 2, \dots, B\}. \quad (24)$$

As a representation value, calculate m_k

$$m_k := b_k + \frac{\delta}{2}, \quad k \in \{1, 2, \dots, B\}. \quad (25)$$

Now define \tilde{Y} and function g as

$$\tilde{Y} := k \Leftrightarrow Y \in B_k, \quad (26)$$

$$g(\tilde{Y}) := m_{\tilde{Y}}. \quad (27)$$

Then, let us define

$$MI\text{-TET} := I(A; \tilde{Y}|S) \quad (28)$$

$$= \mathbb{E}_s \left[I(A; \tilde{Y}|S = s) \right] \quad (29)$$

$$= \mathbb{E}_s \left[\sum_{\tilde{Y}} p(\tilde{Y}|s) D_{KL} \left(p(A|\tilde{Y}, s) || p(A|s) \right) \right]. \quad (30)$$

In short, MI-TET can be interpreted as the conditional mutual information between the action A and the discretized reward signal \tilde{Y} with the conditioning on the state S .

First, one might ask why this discretization process is necessary. The primary motivation is to ensure a robust and computationally simple metric. In many reinforcement learning tasks, the action is often given to be discrete while the Y is often continuous, instead; this is because the reward function R is often taken to be continuous. If we were to use the continuous variable Y directly, calculating the mutual information $I(A; Y|S)$ would first require us to estimate the underlying continuous probability density (e.g. $p(y|a, s)$). This step is not reachable by itself, rather forcing us to employ complex methods like Kernel Density Estimation (KDE), using the captured samples. This adds significant computational overhead for estimating our MI-TET $I(A; \tilde{Y}|S)$, thus making the online tracking process of MI-TET unfeasible.

Moreover, even if Y is given to be discrete, there exist some chances that A and Y might not *match* that well; for instance, Y is already divided into much more segments than A is. This would make the given value of the mutual information become almost near to zero, since only sparse number of samples might be included into each bin of the histogram.

Therefore, we employ a deliberate, a priori discretization of Y into \tilde{Y} . This process is mainly achieved by introducing the bin count B as a crucial hyperparameter. If we set B too large, we replicate the second problem mentioned above: the resulting histogram becomes too sparse, and the estimated mutual information $I(A; \tilde{Y}|S)$ may become vanishingly small. Conversely, if B is set too small (e.g. $B = 1$), \tilde{Y} becomes a constant, and the mutual information trivially becomes zero, losing all the information. Yet, it is still *better than nothing*; by properly selecting B in advance, we aim to adjust the mutual information reasonably interpretable level.

Second, the vast motivation of MI-TET itself. Intuitively, the ultimate goal of reinforcement learning can be simplified into the following one sentence: *Let's increase the volume of what I expect to get by adjusting what I do.* This naturally motivates us to think *What if we just quantify how much information the action distribution itself has about the reward distribution?* and as a mathematical way, one might easily choose mutual information for that purpose. Moreover, it is reinforcement learning-friendly, which almost every of the conventional metrics does not have as a property. There are two words, **exploration** and **exploitation** when we try to summarize the typical reinforcement learning process. Exploration prescribes the agent's behavior where it intentionally attempts a new action randomly to find a better policy, whereas exploitation signifies rather agents concentrating on selecting the most *good looking* behavior learned to date when choosing the new action. In most reinforcement learning processes, the agent first tries exploration for most of the time, while gradually increasing the rate of exploitation with a decrease in the portion of exploration [17]. In the reference [2], we must carefully look at the role of β in the softmax-PQC, which is called an inverse-temperature parameter. This is the very parameter controlling *greediness*, i.e. the dynamic of those two concepts, exploration and exploitation, and in the work the authors said they employed a linear annealing schedule starting from 1 and increasing up to the final β (task-specific, prefixed value). The proposed metric, MI-TET, then can be understood with β , showing the following relationships:

1. **During effective exploration** (low β , stochastic policy), MI-TET should be high.
2. **During exploitation** (high β , policy converges), the agent's policy becomes deterministic, i.e. $\pi(A|S) \rightarrow 1.0$ for the best action. As the policy's action entropy $H(A|S)$ drops to zero, the mutual information $I(A; \tilde{Y}|S)$ must also drop to zero.

Thus by using the MI-TET, one can quantify and track how much the action distribution space the policy spews out narrows and gradually gets ‘concentrated’ over time, which are both quite important in analyzing the learning performance.

B. Theorems on Trainability and Expressivity

What is interesting with this MI-TET is that we can upper bound some values that are related to trainability and expressivity, respectively, with the use of our MI-TET. First, let us introduce some theorems of trainability, which give us the upper bound for the norm of gradients. To do so, one needs to understand what one-shot game is.

Definition 3 (Informal, One-shot game). *One-shot game is basically the same as the case when the finite horizon T is equal to one; that is, the state is fixed for s and the agents picks the action $a \in A$ based on the policy $\pi_\theta(a|s) =: \pi_\theta(a)$. As a result, it gets a reward $R(s, a) =: R(a) \in \mathbb{R}$. Our job is to find an optimal parameter θ^* defined as*

$$\theta^* = \operatorname{argmax}_\theta \mathbb{E}_{a \sim \pi_\theta} [R(a)]. \quad (31)$$

By playing this one-shot, immediate games multiple times, we aim to get closer to the optimal parameter θ^ .*

Our proof for the trainability theorem begins with giving a proof for the simplified version, trainability theorem for just the one-shot game, and inducing that result further to much broader, generalized cases. We even discriminate the easy cases within two subcases, where the one with original Y and discretized \tilde{Y} .

Theorem 1 (Trainability Theorem (1) - One-shot game, non-discretized). *Let our objective function $\eta_s(\theta) := \mathbb{E}[R(a)]$, and define the score function $S_\theta(a)$ as*

$$S_\theta(a) := \nabla_\theta \log \pi_\theta(a). \quad (32)$$

Let $g_s(\theta)$ denote the gradient of our objective function η_s and assume

$$\|g_s(\theta)\| \leq G_{\max}, \quad |R(a)| \leq R_{\max}. \quad (33)$$

Then the following holds:

$$\|g_s(\theta)\| \leq \sqrt{2}G_{\max}R_{\max}\sqrt{I(A; R)}. \quad (34)$$

Note that some notations and MI-TET have changed due to the assumptions of the theorem. If we reach further to the discretized case, we get

Theorem 2 (Trainability Theorem (2) - One-shot game, discretized). *With the same notation given in the Theorem 1,*

$$\|g_s(\theta)\| \leq \sqrt{2}G_{\max}R_{\max}\sqrt{I(A; \tilde{R})} + G_{\max}\Delta. \quad (35)$$

Again note that by discretizing Y , we encounter $G_{\max}\Delta$ as a cost. Yet, we take the \tilde{Y} for the real MI-TET, due to the the reasons given earlier.

Next is our main trainability theorem. According to that, MI-TET has shown to be able to work as an **upper bound** for our modified (scaled) objective function's gradient; hence a trainability measure. Remark that when we measure our policy function (or circuit)'s trainability or keep tracking on it, we

Theorem 3 (Trainability Theorem (3) - Multiple games, discretized). *Assume $|Y| \leq Y_{\max}$, and let*

$$\eta'(\theta) := \frac{1-\gamma}{1-\gamma^T} \eta(\theta) = \frac{1-\gamma}{1-\gamma^T} \mathbb{E} \left[\sum_{t=0}^T \gamma^t R_t \right]. \quad (36)$$

Then

$$\|\nabla_{\theta} \eta'(\theta)\| \leq \sqrt{2} G_{\max} Y_{\max} \sqrt{I(A; \tilde{Y}|S)} + G_{\max} \Delta, \quad (37)$$

where $Y \in \{G_t, Q^{\pi_{\theta}}\}$. In a big-oh type notation,

$$\|\nabla_{\theta} \eta'(\theta)\| \leq O\left(\sqrt{I(A; \tilde{Y}|S)}\right). \quad (38)$$

use the modified objective function's gradient $\nabla_{\theta} \eta'(\theta)$. On the other hand, for the real update process, we use the information of the original objective function's gradient $\nabla_{\theta} \eta(\theta)$. In one sentence,

$$\|\nabla_{\theta} \eta'(\theta)\| \leq O\left(\sqrt{I(A; \tilde{Y}|S)}\right) = O(\sqrt{\text{MI-TET}}) \quad (39)$$

while also

$$\|\nabla_{\theta} \eta(\theta)\| \leq O\left(\sqrt{I(A; \tilde{Y}|S)}\right) = O(\sqrt{\text{MI-TET}}). \quad (40)$$

For the complete proof of these trainability theorems, please refer to the Appendix A.

Next, we discuss the concept of expressivity. As we have seen in the earliest sections, novel, standard definition adapted to the reinforcement learning framework to account for its inherent temporal properties should be given in advance to start the discussion. We, therefore, first propose its intuitive definition: the policy function's expressivity as the **deviation** among multiple sampled action distributions.

Definition 4 (Definition of Expressivity in RL). *Fix a state s and let $Z \in \{1, 2, \dots, N\}$ denote the latest N numbers of samplings' indices. Define*

$$\pi_i^s(a) := P(A = a | Z = i, S = s), \quad (41)$$

$$w_i(s) := P(Z = i | S = s) \left(\text{where } \sum_i w_i(s) = 1 \right), \quad (42)$$

and also the mean distribution of A as

$$\bar{\pi}^s(a) := \sum_{i=1}^n w_i(s) \pi_i^s(a) = P(A = a | S = s). \quad (43)$$

Using these two distributions, calculate some **divergence metrics** and define the expressivity in RL as

$$\text{Expr} := \mathbb{E}_{S \sim d_{\pi}} [\text{Divergence Metric}]. \quad (44)$$

As a candidate for that divergence metric, one might choose one of the following:

- *Jensen-Shannon Divergence*

$$JSD_{w(s)}(\{\pi_i^s\}) := \sum_{i=1}^n w_i(s) D_{KL}(\pi_i^s || \bar{\pi}^s) \quad (45)$$

$$= I(A; Z | S = s). \quad (46)$$

- *L2 Divergence*

$$D_2(Z | s) := \sum_i w_i(s) \|\pi_i^s - \bar{\pi}^s\|_2^2. \quad (47)$$

- *TV Divergence*

$$D_{TV}(Z | s) := \sum_i w_i(s) TV(\pi_i^s, \bar{\pi}^s)^2. \quad (48)$$

We are now able to calculate the expressivity of a given policy function in a sampling-based manner, which also enables us to track it. Note that it is finally averaged through arbitrary state s . Then our expressivity theorem is given as follows.

Theorem 4 (Expressivity Theorem). *For those three divergence metrics (Jensen-Shannon Divergence, L2 Divergence, TV Divergence),*

$$\text{Expr} \leq O(\text{MI-TET}) \quad (49)$$

under the condition of

$$I(A; Z | \tilde{Y}, S) = 0 \text{ (or } \simeq 0\text{).} \quad (50)$$

The assumption $I(A; Z | \tilde{Y}, S) \simeq 0$ means that, given the state and (discretized) reward, the policy's action distribution does not depend on the temporal index Z ; i.e., the policy is *locally* stationary under comparable state-reward conditions. Then the theorem says that under this regime, MI-TET would serve as a valid upper bound for our expressivity metric. For the proof of this expressivity theorem, please refer to the Appendix B.

C. Sample-based Estimation of MI-TET

Recall that our MI-TET is defined as

$$I(A; \tilde{Y}|S) = \mathbb{E}_{s \sim d^\pi} [D_{KL}(p(a, \tilde{y}|s) || p(a|s)p(\tilde{y}|s))] \quad (51)$$

$$= \sum_s d^\pi(s) \sum_{a, \tilde{y}} p(a, \tilde{y}|s) \log \frac{p(a, \tilde{y}|s)}{p(a|s)p(\tilde{y}|s)}. \quad (52)$$

If the state is continuous, then the first summation would instead be an integral.

Yet, it is not suitable for sample-based estimation when considering the case of a **large state space**, which is quite common in most reinforcement learning applications. If so, it is highly unlikely that the agent revisits already visited states, thus gathering only somewhat ‘sparse’ datasets. To faithfully estimate the theoretical value of MI-TET in a given environment, one must estimate

$$I_s = \sum_{a, \tilde{y}} p(a, \tilde{y}|s) \log \frac{p(a, \tilde{y}|s)}{p(a|s)p(\tilde{y}|s)} \quad (53)$$

for each state $s \in S$ in a sampling-based manner. In those ‘sparse’ settings, the estimated values of $p(a, \tilde{y}|s)$, $p(a|s)$, and $p(\tilde{y}|s)$ would be close to zero, thus making the entire estimation unstable, with high variance and bias. Thus, although informal, one might understand our MI-TET is susceptible to the curse of dimensionality as well: to make the value interpretable, one would have to gather *exponentially* many samples. However, gathering sufficient samples is always a difficult task.

Therefore, we need a metric that we can use instead of MI-TET while also sharing the key essence of it. We argue that $I(A; \tilde{Y})$, which is not conditioned by the state S , might be able to serve that desired role. Reasons are the following. First,

$$I(A; \tilde{Y}, S) = I(A; S) + I(A; \tilde{Y}|S), \quad (54)$$

$$I(A; \tilde{Y}, S) = I(A; \tilde{Y}) + I(A; S|\tilde{Y}) \quad (55)$$

which is trivial considering the definition of mutual information. Then we get those two equations:

$$I(A; \tilde{Y}|S) = I(A; S|\tilde{Y}) + I(A; \tilde{Y}) - I(A; S), \quad (56)$$

$$\Delta := I(A; \tilde{Y}|S) - I(A; \tilde{Y}) = I(A; S|\tilde{Y}) - I(A; S), \quad (57)$$

where Δ denotes the ‘gap’ between those two metrics. We know in advance that we can upper bound the mutual information by the entropy, thus yielding again

$$I(A; \tilde{Y}) - I(A; S) \leq I(A; \tilde{Y}|S) \leq I(A; \tilde{Y}) + H(S|\tilde{Y}) \quad (58)$$

or by using gap Δ ,

$$-I(A; S) \leq \Delta \leq H(S|\tilde{Y}). \quad (59)$$

Let us consider the scenario where those ‘desired’ two conditions hold: $I(A; S) \approx 0$ and $H(S|\tilde{Y}) \approx 0$. The first condition, $I(A; S) \approx 0$, describes a situation where the policy

$\pi(A|S)$ is nearly independent of the state S . It is a condition that can be observed at two distinct phases of reinforcement learning.

First, during the early states of learning (i.e., exploration), the agent’s policy is often initialized to near-uniform. Since the action is chosen almost randomly regardless of the state, the state S provides little information about the action A , resulting in $I(A; S) \approx 0$.

Second, during the late stages of learning (i.e., exploitation). As learning proceeds, the agent may learn that a single action is globally optimal and more beneficial than all others, independent of the observed state. As the agent increases its rate of exploitation, it may converge on a policy that almost always selects this dominant action. This effectively makes the policy output deterministic (e.g., $\pi(A|S) \approx \pi(A)$ for all S), again rendering it independent of the state and causing $I(A; S) \approx 0$. However, although the first situation is widely seen in most of RL tasks, the second case does not hold for all, thinking of the cases where the states are much more ‘distinct’ and thus require considerably ‘distinct’ actions suitable just for that state; in these environments, analyzing $H(A|S) = E_s [H(A|S = s)]$ would be much more important (for instance, CartPole).

Meanwhile, the second condition, $H(S|\tilde{Y}) \approx 0$ is a bit more non-intuitive. It reads that \tilde{Y} , which is actually a reward signal of the environment, should explain much of the state S . Excessively, the entropy would be zero when S can be described as a function of \tilde{Y} . But this is an *environment-related* issue: some environment might satisfy that, while others do not. We can think of specific learning environments where the reward indicates the ‘progress’ of learning, such as a *maze*: the agents solves the maze while earning a reward as a distance of the current position and the end point. In such a setting, we can evaluate the current progress based on the earned reward to certain extent, observing a correlation of current state and the reward. However, as we mentioned earlier, since it is a problem-specific issue, we can conclude that our estimator $I(A; \tilde{Y})$ has some probabilities that it *overestimates* the value of $I(A; \tilde{Y}|S)$, when our desired second condition fails to hold.

Although $I(A; \tilde{Y})$ contains some concerns and issues, it is almost only computationally feasible option that shares the key idea of MI-TET, which is the **ability to track the dynamics of learning**. We know that

$$I(A; \tilde{Y}) \leq H(A). \quad (60)$$

During the exploration phase, $H(A)$ is high, allowing $I(A; \tilde{Y})$ to be non-zero. As the agent shifts to exploration, the policy converges, $H(A)$ trends to zero, and consequently, $I(A; \tilde{Y})$ is forced to trend to zero as well. This observation aligns with the theoretical rationale underlying the definition of MI-TET presented earlier. Thus, we posit $I(A; \tilde{Y})$ as a notable, computationally viable heuristic for observing the temporally variable alignment of policy and reward, which is the very property we desire.

Moreover, it is also crucial to note that this same challenge of state-space dimensionality applies directly to the practical estimation of our proposed Expressivity metric, $Expr =$

$\mathbb{E}_{S \sim d_\pi} [I(A; Z|S)]$ (if we just use JSD divergence). Just as estimating $p(a, \tilde{y}|s)$ is intractable for large state spaces, so too is estimating the state-conditioned policy distributions $\pi_i^s(a) = P(A = a|Z = i, S = s)$ required for the JSD calculation. Therefore, to maintain a consistent and computationally feasible methodology, we also adopt the unconditioned mutual information, $I(A; Z)$, as the practical, sample-based proxy for our Expressivity metric in the subsequent numerical analysis.

D. Numerical Simulations

To substantiate our theoretical findings presented in the previous sections, we now conduct a series of numerical simulations. The primary objective of this section is to provide empirical validation for the core claims of our Mutual Information-based Expressivity and Trainability (MI-TET) metric, specifically focusing on its computationally feasible proxy, $I(A; \tilde{Y})$. We utilize the standard CartPole-v0 reinforcement learning environment, which provides a clear, discrete action space suitable for observing the learning dynamics we have discussed [18]. As stipulated in our methodology, we employ the REINFORCE algorithm with the normalization technique, implemented by the reuploading-based parameterized quantum circuit (PQC) architecture proposed by *Jerbi et al.* [2].

Our experimental investigation is structured to answer the following key questions sequentially:

1. **Validation of Temporal Dynamics:** First, we demonstrate that our proxy metric $I(A; \tilde{Y})$ dynamically tracks the agent’s learning progression. We verify that its behavior correctly reflects the crucial transition from the high-entropy exploration phase to the low-entropy exploitation phase, a fundamental characteristic of the RL process that conventional static metrics fail to capture. More practically, we measure the average policy entropy, $H(A|S)$, to compare our metric $I(A; \tilde{Y})$ with the degree to which the policy itself has become deterministic.
2. **Empirical Verification of Theorems:** Second, we provide direct empirical evidence for our main theoretical contributions. We test the **Theorem 3 (Trainability Theorem)** by simultaneously tracking $I(A; \tilde{Y})$ and the norm of the total gradient ($\|\nabla_\theta \eta'(\theta)\|$), validating the derived upper-bound relationship. Concurrently, we test the **Theorem 4 (Expressivity Theorem)** by comparing the MI-TET proxy $I(A; \tilde{Y})$ against our sample-based temporal expressivity metric—specifically, its practical proxy $I(A; Z)$ —to confirm the theorized upper-bound relationship holds for these feasible estimators.
3. **Demonstration of Practical Utility:** Finally, we illustrate the practical utility of MI-TET as an ‘easy criterion’ for model (PQC structure) selection. We evaluate three distinct PQC architectures to comprehensively explore the trade-offs between trainability and expressivity:

- (a) **A ‘shallow’ PQC (1 layer):** Expected to be trainable but limited by low expressivity
- (b) **A ‘default’ PQC (5 layers):** Expected to be both trainable and sufficiently expressive (our baseline).
- (c) **A ‘deep-BP’ PQC (10 layers):** Expected to have high expressivity but suffer from low trainability (e.g., Barren Plateaus).

We show that our $I(A; \tilde{Y})$ proxy effectively distinguishes these three scenarios. It provides an early-stage indicator not only for identifying a failure of trainability but also for diagnosing insufficient expressivity, long before the convergence of the final reward.

We also implement two key modifications to the training procedure to ensure stable and efficient learning.

First, to explicitly manage the exploration-exploitation trade-off, we employ a linear annealing scheduler for the inverse temperature parameter, β , which controls policy greediness as discussed in the earliest section. Unlike the fixed parameter used in the original work [2], our β is initialized at 1.0 and linearly increased to a final value of 1.5 over the total number of training batches. This gradually shifts the agent’s policy from an initial exploratory phase to more deterministic, exploitative phase.

Second, to detect training failure and avoid unnecessary computation, we introduce a patience-based early stopping criterion. We monitor the average rewards over a 10-batch sliding window. If the average reward of the latter 5 batches within this window drops below the average reward of the preceding 5 batches, we consider the policy to have collapsed and terminate the run prematurely.

1. Validation of Temporal Dynamics

First, as mentioned earlier, choosing an appropriate bin count B is important: too small a value can lead to ‘underfitting’, while too large a value may cause ‘overfitting’, both of which hurt the interpretability of MI-TET. Therefore, we evaluated several candidate values and present MI-TET’s sensitivity to them. Practically, we tried 2, 5, 10, 20, 50 as them and saw the relationship in Figure 1. The figure illustrates that the MI-TET value itself can be scaled substantially as the bin count changes. Prior to computing the actual values, we expected that a large bin count such as 50 would fall into the overfitting regime discussed earlier, thereby yielding a smaller MI-TET value. However, the empirical results indicate that the case of 50 bins is still within the progression from an underfitting regime toward the ‘sweet-spot’ region, rather than going beyond it. We guess that if the bin count were increased even further, MI-TET would eventually exhibit an increase followed by a decrease, consistent with the typical trend of overfitting emerging at sufficiently large bin resolutions.

Note that computing MI-TET requires information associated with the learning status—such as the information of the ‘chosen’ actions and the resulting rewards. Because training

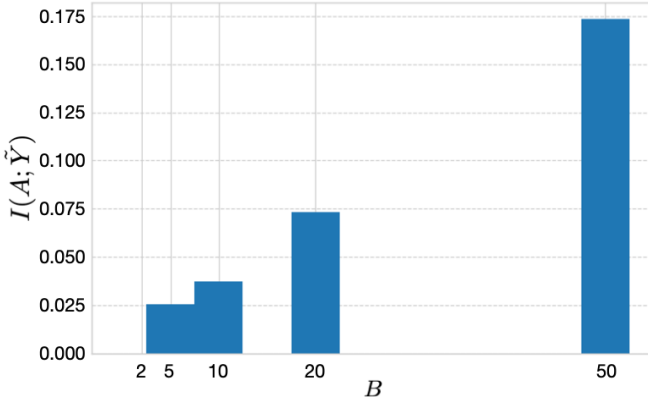


FIG. 1: **Sensitivity of MI-TET to the bin count B .** Using the captured learning information in the first batch of learning (i.e., actions and earned rewards), we evaluated MI-TET upon multiple choice of bin count 2, 5, 10, 20, 50.

was conducted in batches, our theoretical expectation is that MI-TET should decrease as the batches progress, implying that the value should be largest in the first batch. For this reason, we computed the sensitivity results using the data from the first batch. In later batches, regardless of the bin count chosen, the MI-TET values would be almost uniformly small, making its sensitivity on the bin count less discernible. Indeed, this anticipated behavior is confirmed and explicitly observed in the experiments presented later in this work.

Since the most appropriate bin count is the one that retains as much information as possible—equivalently, the one that yields a sufficiently large MI-TET value while remaining interpretable—the figure provides empirical justification for choosing a bin count of 50. Accordingly, all subsequent experiments report results based on this choice. To further illustrate how MI-TET’s predictive performance and the tightness of its bounds vary qualitatively with different bin counts, we provide additional results for the case of $B = 10$ in Appendix C.

Next, the overall learning progress of the three cases: the *default* one (layer = 5), the *shallow* one (layer = 1), and the *deep_BP* one (layer = 10). First, the *shallow* case demonstrates that learning fails to begin in any meaningful way and remains confined within a narrow reward range (0-30). Moreover, the fact that the learning curve terminates around episodes 100-150 indicates that early stopping was triggered according to our predefined criterion, further confirming the inadequacy of the shallow PQC. Given that the shallow configuration corresponds to a PQC with only a single reuploading layer, this behavior suggests that its extremely limited expressivity prevents the model from representing sufficiently diverse policy functions, ultimately hindering effective learning.

In contrast, when comparing the *deep_BP* configuration with the *default* setting, we initially expected that *deep_BP*—owing to its higher expressivity—would suffer significant losses in trainability and therefore struggle to learn effectively. Yet, the learning curve suggests that *deep_BP* may, in some

sense, appear to perform better than the default case. Nevertheless, a closer examination reveals that this is not necessarily the case: *deep_BP* exhibits substantially higher variance than the default configuration, particularly around episodes 150-200, and when the learning process enters the final fine-tuning stage, its plateau settles roughly 10 reward points lower than that of the default case. These observations indicate that *deep_BP* cannot be considered unequivocally superior.

More fundamentally, reinforcement learning is inherently stochastic, and it is generally reasonable to assume that a model with roughly twice as many layers—as in the *deep_BP* configuration—would naturally incur greater trainability losses. Therefore, although the learning trend alone may introduce some ambiguity, we regard the default configuration as the reliably trained case, while *deep_BP* despite occasional strong performance, ultimately exhibits weaker trainability as reflected in its instability and lower final plateau. Our subsequent discussion proceeds from this interpretation.

We now turn to demonstrating that MI-TET accurately captures the evolution of the policy function as learning progresses—specifically, the transition from exploration to exploitation and the corresponding change in the underlying action distribution. Since we impose a linear annealing schedule on the temperature parameter β , increasing it from 1.0 to 1.5, it is externally evident that the policy entropy $H(A|S)$ should decrease from the fully uniform value $\log 2 \approx 0.693$ toward zero. Thus, what remains is to verify that MI-TET follows this theoretically expected trend in a consistent manner.

Figure 3 shows that, for all PQC settings, the policy entropy initially increases slightly—reflecting an early exploration phase in which the agent tests policies whose action distributions are close to uniform. As training progresses, however, the agent gradually enters the exploitation regime, and the entropy correspondingly decreases. Although MI-TET does not perfectly capture the initial rise in exploration, it nonetheless exhibits a clear trend: as learning proceeds and the policy becomes more deterministic, MI-TET also decreases in a steady manner.

The *shallow* case does not display this behavior as clearly, but this is expected: as seen in Figure 2, shallow corresponds to an early-stopped configuration that likely never reached the point where MI-TET begins to meaningfully track the underlying policy dynamics. This further supports the interpretation that the absence of the expected trend in the shallow case is a natural consequence of insufficient training progress.

This relationship becomes even more evident when examining the correlations between MI-TET and policy entropy. With the exception of the shallow case—which shows only a weak correlation of -0.18—the *default* and *deep_BP* cases exhibit **strong positive correlations** of 0.72 and 0.80, respectively. These results further affirm that MI-TET reliably reflects the entropy dynamics of the learned policy. (All correlation matrices are provided in Appendix D.)

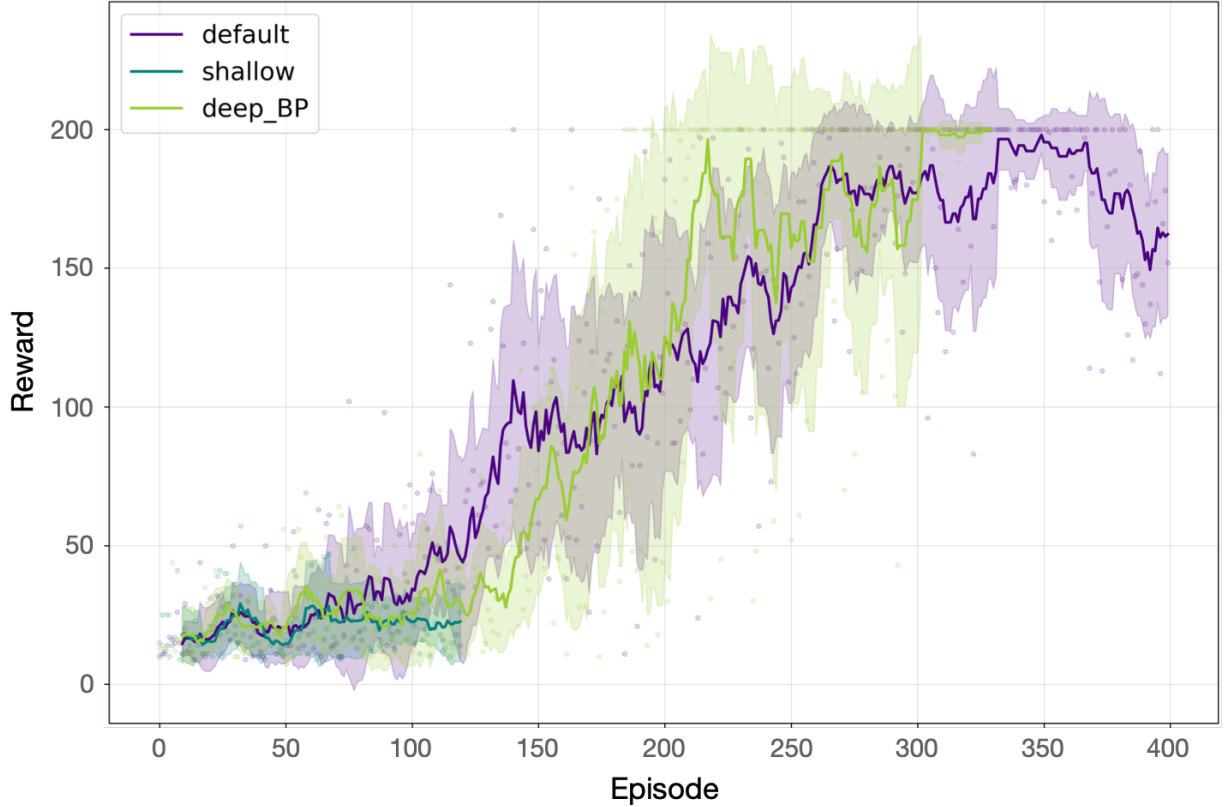


FIG. 2: **Overall learning progress of the total tree cases: *default*, *shallow*, *deep_BP*.** Each colored point represents the actual reward obtained in each batch for a given PQC setting, while the corresponding bold colored line indicates the 10-batch moving average of the reward for that setting.

2. Empirical Verification of Theorems

Now we turn to the phase of validating our two core theorems: the trainability theorem and the expressivity theorem. Again, note that we have utilized two proxies $I(A; \tilde{Y})$ (for the original MI-TET) and $I(A; Z)$ (for the original expr with JSD) here in total.

First, we propose raw data of our three PQC settings, which is the following Figure 4. The gray area in the plot signifies the region where our MI-TET works as an appropriate upper bound, whereas the red area serves as the opposite. It is important to note that the theoretical analysis only established that both $\sqrt{\text{MI-TET}}$ and MI-TET can upper-bound the gradient norm and the expressivity metric respectively, in the big-O sense. In Figure 4, however, no constant factors have been multiplied or added to MI-TET; therefore, the presence of small ‘red’ regions where the bound appears violated is naturally expected. In general, for MI-TET to serve as a proper upper bound in practice, one would normally estimate an appropriate scaling constant from the accumulated learning data and multiply MI-TET by that constant. Remarkably, for the experiment with a bin count of 50, the theorem is empirically validated even without applying such a correction: the raw MI-TET already behaves as a valid upper bound.

This behavior does not appear when the bin count is set to 10, as shown in Appendix C. Under those conditions, the raw

MI-TET no longer aligns with the expected bound, and estimating and applying a scaling constant at intermediate stages of learning becomes essential for MI-TET to function properly as an upper bound. The contrast between the two setting strongly suggests again that **choosing a sufficiently large bin count is critical for ensuring adequate resolution when using MI-TET**.

Visually, one can also observe a notable correlation between MI-TET and both the gradient norm and expressivity. This observation is quantitatively supported by the correlation matrices provided in Appendix D. Although the correlation between the gradient norm and MI-TET appears noticeably weaker than that between expressivity and MI-TET, this observation is entirely natural. Policy-gradient methods are known to exhibit inherently high variance in their gradient estimates, and no additional baseline techniques, such as value function approximators were applied in our simulation. Consequently, a direct correlation with the raw gradient norm is not necessarily the most meaningful metric. More precisely, one should instead consider the underlying trend of the gradient—namely, an implicit trajectory that smooths out its fluctuations—and assess the extent to which MI-TET tracks this trend. From this perspective, the weaker apparent correlation is expected, and the qualitative alignment between MI-TET and the gradient’s trend remains a more appropriate point of evaluation.

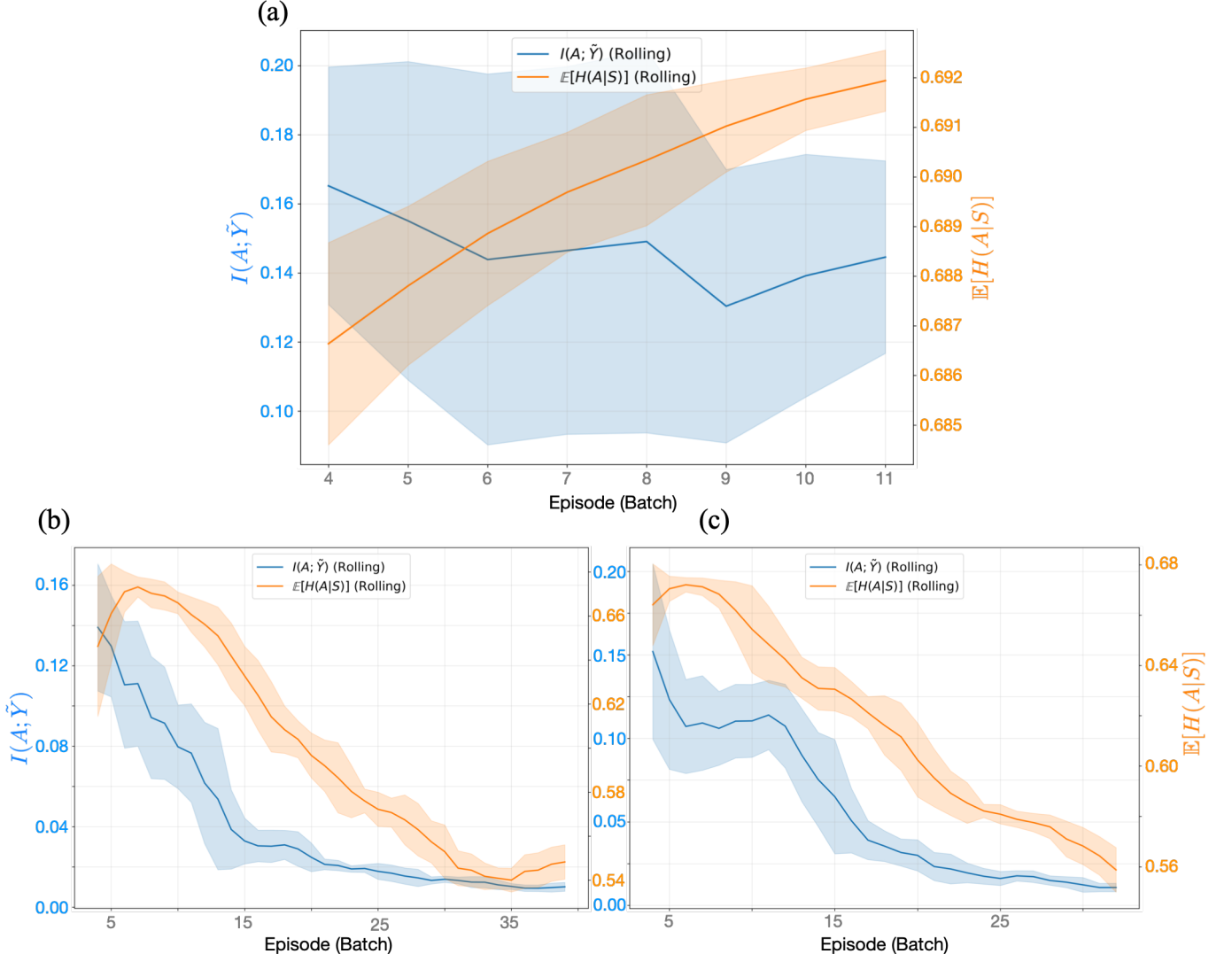


FIG. 3: Comparison of MI-TET trends for the three configurations with the policy entropy $H(A|S)$: (a) Shallow, (b) Default, and (c) Deep_BP.

3. Demonstration of Practical Utility

Finally, we now examine how the early-phase MI-TET trends can be used to infer which structure is likely to effectively and stably achieve the highest long-term expected reward. Figure 5 presents the MI-TET values across episodes for the three configurations. As established earlier, we already know that the *moderate (default)* configuration yields the best overall performance among the three. Thus, our main goal then transfers to the task of distinguishing both *low-expressive* and *overly expressive* PQCs from this optimal *moderate* case through MI-TET.

For the *low-expressive* PQC, MI-TET exhibits extremely high variability and fails to converge, even by episodes 100-150, instead maintaining persistently large and unstable values. When considered together with the previously discussed relationship between MI-TET and policy entropy, this implies

that the underlying policy function has not stabilized and remains far from convergence; and our MI-TET directly captures it as some ‘early warning’. Thus, we would be able to argue that **the persistent lack of convergence and high fluctuation in MI-TET naturally characterize the behavior of a PQC with insufficient expressivity, in a high likelihood sense.**

In contrast, distinguishing between the moderate and the overly expressive (deep) configurations is less straightforward. As previously observed in the learning curves, both settings achieve similarly favorable trends, and their MI-TET trajectories also overlap substantially across many portions of training. Therefore, unlike the low-expressive PQC, which MI-TET clearly identified, these two higher-capacity models cannot be separated based on the simple global patterns alone.

However, certain notable differences emerge when focusing on learning stability. For the moderate-depth model, although it shows sharp fluctuations during the earliest periods

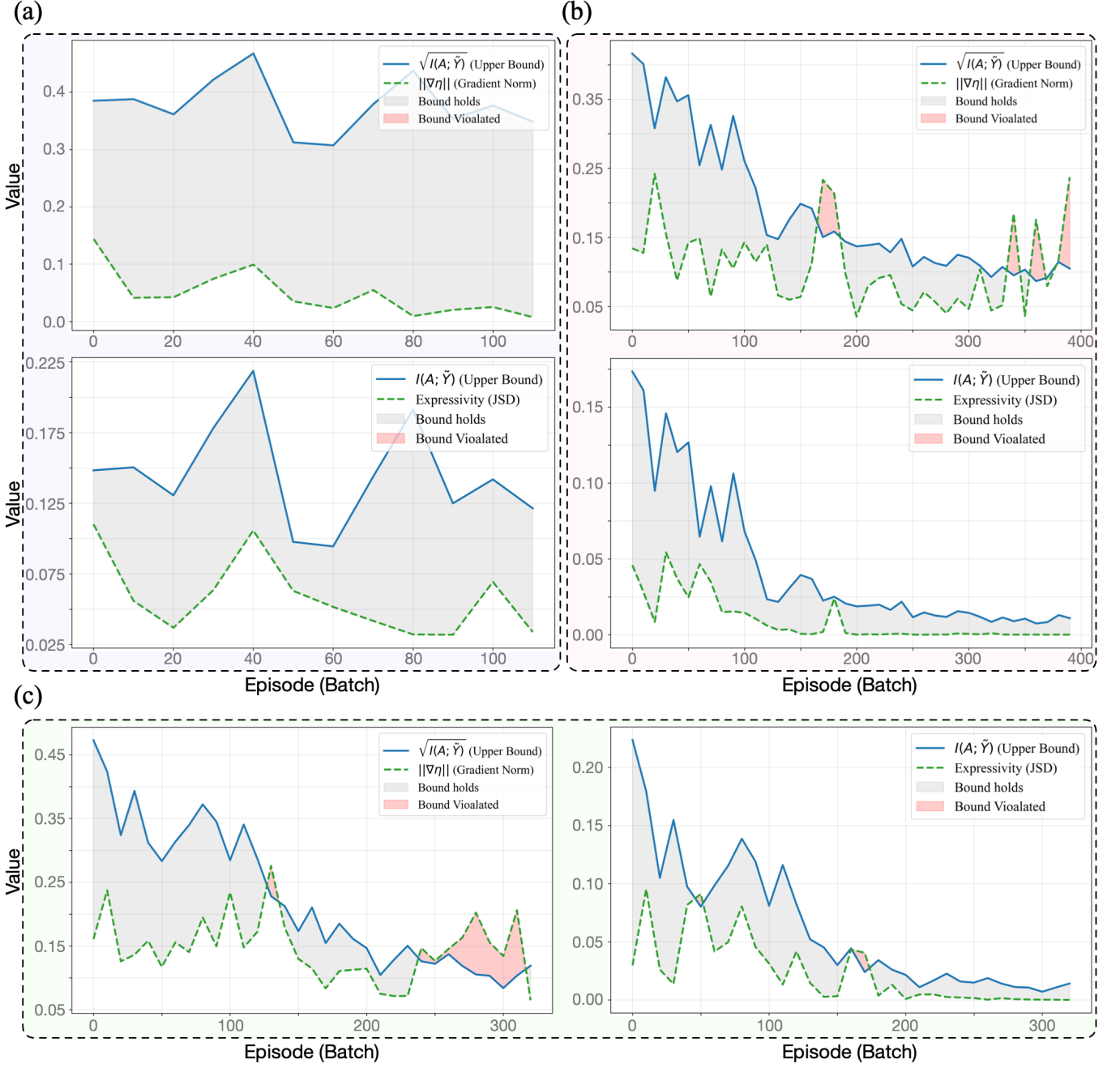


FIG. 4: **Theorem validation with the different PQC structure.** Note that these are literally ‘raw’ data, without any scaling factor is multiplied to both $I(A; \tilde{Y})$ and $\sqrt{I(A; \tilde{Y})}$: (a) Shallow, (b) Default, and (c) Deep_BP.

(0-40), it stabilizes thereafter and exhibits a relatively smooth decline of MI-TET toward zero. In contrast, the deep configuration shows pronounced fluctuations around episodes 30-50 and again near episodes 150-200. (What we refer to as ‘sharp’ or ‘pronounced’ changes here correspond to variations on the order of the vertical tick size 0.01.)

Interestingly, these two fluctuations periods coincide with the regions in Figure 2 where the deep model exhibited larger reward variance than the moderate model. Recall our earlier

interpretation: deep PQCs can suffer not only from gradient vanishing (i.e., barren plateaus) but also from *relative* gradient exploding where the magnitudes of the update gradients become disproportionately large. This phenomenon produces the greater variance, which we empirically observed in the reward logs, and ultimately harms trainability compared to the moderate-depth model. The present MI-TET trends reflect the same mechanism: the sudden spikes and unstable segments in the deep configuration correspond to episodes where gradient-

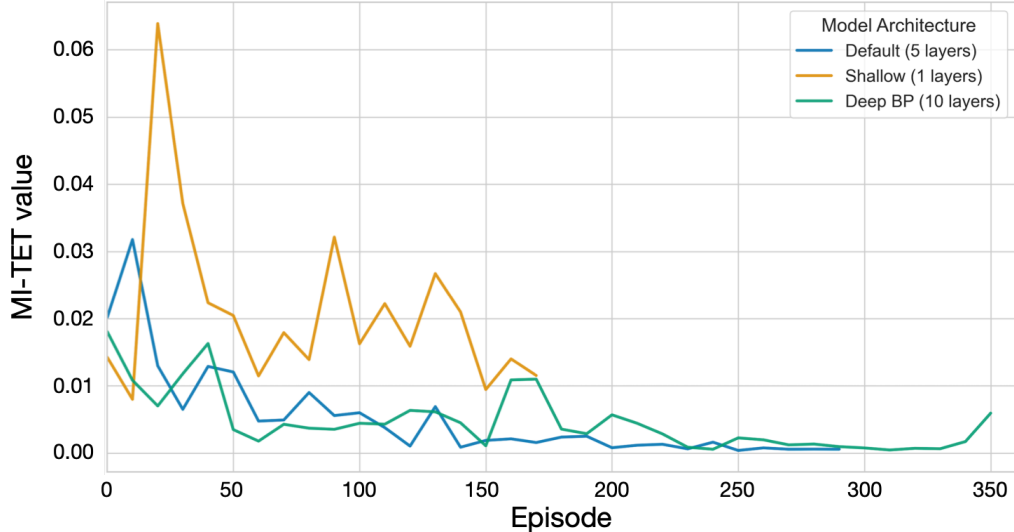


FIG. 5: MI-TET values per episodes with the three given PQC structures.

related instability emerges.

Hence, although with somewhat lower confidence than in the earlier comparison, **the deep configuration can be characterized by occasional, noticeable surges in MI-TET that exceed natural threshold during training.** These spurts signify underlying instability in the update dynamics, suggesting that MI-TET can partially serve as an indicator of trainability. This concept becomes even clearer in later stages of training: as shown in the Figure 8, the gradient norm for the deep PQC begins to rise again around the episode 350, and remarkably, MI-TET exhibits a similarly abrupt increase in that region. While such qualitative signals do not actually satisfy our initial goal of identifying the optimal PQC solely from early MI-TET observations, they nevertheless provide strong evidence that MI-TET reflects aspects of trainability with surprising fidelity.

IV. CONCLUSION AND FUTURE WORKS

A. Summary and Value of Findings

In this work, we identified expressivity and trainability as two essential indicators in quantum reinforcement learning—particularly in quantum policy gradient methods—and point out that no existing, conventional metric simultaneously captures both in a manner aligned with the nature of (quantum) reinforcement learning. To address this gap, we introduced a new definition of expressivity based on *how the action distribution produced by a policy function evolves over time*. We showed that the state-conditional mutual information between the discretized reward signal and the action distribution upper-bounds this notion of expressivity and the total gradient norm. We further hypothesized that this mutual information metric (MI-TET) is well-suited to capturing one of the defining characteristics of reinforcement learning: the exploration-

exploitation trade-off. Our simulations in the CartPole environment confirm this prediction. Additionally, MI-TET effectively reflects trainability-related behaviors such as increased reward variance due to *relative* gradient exploding and phenomena like gradient re-increasing. The consistently strong correlation observed between MI-TET and expressivity further substantiates that MI-TET serves as a unified metric providing simultaneous insight into both trainability and expressivity. In other words, MI-TET has clear potential as an indicator of stable learning convergence and as a practical tool for predicting and comparing the performances of different PQC architectures. Indeed, our experiments show that MI-TET reliably detects non-convergence or divergence in low-expressive settings, as well as unstable spikes in overly expressive regimes.

The value of the proposed MI-TET becomes even more pronounced in environments with *sparse or delayed rewards*. A sparse and delayed reward environment refers to a setting where the agent receives meaningful rewards only at the very end of an episode—or, in less extreme cases, receives nonzero rewards only at irregular and infrequent time steps, with all remaining rewards being near zero. Such environments often provide the agent with *unspecified* reward signals: it becomes unclear whether a given positive reward was obtained because the agent discovered a meaningful underlying structure through its actions or merely due to accidental success. This ambiguity poses a fundamental challenge to generalization capabilities of reinforcement learning agents [19]. As such, reward sparsity has long been recognized as a major noble obstacle for conventional reinforcement learning methods and continues to motivate active research on various mitigation strategies [20–22].

In such environments, it becomes exceedingly difficult—if not possible—to determine in the early stages of training whether learning is actually progressing when relying solely on episodic returns or moving-average rewards, as is commonly done. In contrast, the essence of MI-TET lies in the

mutual information between two distributions; rather than depending on the absolute magnitude of rewards, it directly captures *the extent to which actions explain the observed reward patterns*.

More concretely, because we theoretically established that the gradient norm and temporal expressivity are upper-bounded by MI-TET, any moment at which MI-TET departs meaningfully from zero can be interpreted as a point where non-trivial gradients are flowing—i.e., a point where actual learning is taking place. Conversely, when MI-TET remains close to zero, this might indicate that gradients have effectively vanished and learning has stagnated. Even in sparse-reward settings, occasional reward events inevitably induce statistical dependence between those rewards and the corresponding action patterns, and MI-TET directly reflects this. As a result, the progress of learning can often be continuously monitored through MI-TET even when the agent receives predominately uninformative, near-zero rewards.

Furthermore, when MI-TET is computed through a simple proxy, it does not require any environment-specific information beyond what is already available to the agent—namely, the observed rewards and the agent’s own actions. Since no state information or external environmental knowledge is needed, MI-TET would be able to cope with fully black-box setting and is therefore a strong candidate for a robust learning-progress tracker in environments characterized by sparse rewards.

B. Future Directions and Open Questions

This work has several limitations that naturally suggest directions for future research. First, our expressivity theorem is theoretically meaningful only under the additional assumption that a certain mutual information term $I(A; Z|\tilde{Y}, S) \approx 0$. A promising line of future work is to relax this condition—either by refining the expressivity notion introduced in this study while preserving its core intuition, or by modifying the definition of MI-TET itself—so that comparable bounds can be derived without relying on such a strong assumption.

Second, due to the curse of dimensionality in large state spaces, we were forced to replace the state-conditional quantities $I(A; \tilde{Y}|S)$ and state-averaged expressivity $I(A; Z|S)$ with unconditional proxies $I(A; \tilde{Y})$ and $I(A; Z)$, which can be estimated more robustly from finite samples. While this makes MI-TET and the associated expressivity metric practically usable, it also blurs their original state-dependent interpretation. Future work may therefore seek either more sample-efficient ways to mitigate the curse of dimensionality—so that genuinely state-conditional versions of MI-TET become estimable—or alternative proxies that track the same temporal phenomena with tighter theoretical control.

Beyond these limitations, several more ambitious extensions are possible. One natural direction is to promote MI-TET to a fully quantum quantity and evaluate it directly on quantum hardware. In our current framework, MI-TET is defined in terms of classical mutual information between the ac-

tion and reward-signal distributions, estimated from sampled trajectories. In a genuinely quantum reinforcement learning setting, however, the action register, the environment’s response and even the reward encoding can all be treated as quantum systems. One could then define a ‘quantum MI-TET’ based on quantum mutual information between suitable subsystems, expressed via von Neumann entropies, and estimate it using quantum neural techniques such as QMINE, which leverages the quantum Donsker-Varadhan representation to learn von Neumann entropy and quantum mutual information from data [23]. Embedding the variational quantum policy and reward-bearing environment into a joint quantum state and training a QMINE-style estimator alongside policy optimization would enable monitoring of trainability and temporal expressivity directly in the quantum domain, which would be a nice and interesting open direction from this work.

Another promising avenue is to couple MI-TET with quantum resource measures, thereby moving toward resource-aware quantum reinforcement learning. In distributed quantum scenarios, where the agent and environment reside a separate quantum nodes connected by constrained quantum channels, an effective policy should not only achieve high expected reward but also respect limitations on communication and entanglement. Quantum uncommon information—operationally define as the minimal quantum communication cost required to exchange two quantum states—provides a natural notion of such a cost, and recent work has proposed QDVR-based neural estimators for upper and lower bounds on this quantity [24]. Combining these tools, one can envision a multi-objective quantum RL framework in which MI-TET serves as a information-theoretic indicator of learnability and temporal expressivity, while neural estimates of quantum uncommon information quantify the communication resources consumed by the policy.

V. ACKNOWLEDGEMENT

This work was supported by the National Research Foundation of Korea (NRF) through a grant funded by the Ministry of Science and ICT (Grants Nos. RS-2025-00515537 and RS-2023-00211817), the Institute for Information & Communications Technology Promotion (IITP) grant funded by the Korean government (MSIP) (Grants Nos. RS-2025-02304540 and RS-2019-II190003), the National Research Council of Science & Technology (NST) (Grant No. GTL25011-000), and the Korea Institute of Science and Technology Information (Grant No. P25026).

DATA AVAILABILITY

The code and data used in this work are available at the following GitHub link: <https://github.com/absolute-injury/MI-TET/tree/main>

DECLARATION OF COMPETING INTEREST

The authors declare that they have no known competing financial interests or personal relationships that could have appeared to influence the work reported in this paper.

AUTHOR CONTRIBUTION

J.J. contributed to this work, undertaking the primary responsibilities, including the development of the main ideas, mathematical proofs, initial drafting, and revisions of the paper. D.J., J.R. and K.J. provided valuable feedback in shaping the core ideas and overall direction of the work, while K.J. also supervised whole research. All authors discussed the results and contributed to the final paper.

[1] Andrew Ng and Tengyu Ma. CS229 Lecture Notes. Stanford University, 2023. Available at https://cs229.stanford.edu/main_notes.pdf.

[2] Sofiene Jerbi, Casper Gyurik, Simon C. Marshall, Hans J. Briegel, and Vedran Dunjko. Parametrized Quantum Policies for Reinforcement Learning. *NeurIPS 2021*, 2021. Available at <https://arxiv.org/abs/2103.05577>.

[3] Sukin Kim, Peter D. Johnson, and Alán Aspuru-Guzik. Expressibility and Entangling Capability of Parameterized Quantum Circuits for Hybrid Quantum-Classical Algorithms. *Advanced Quantum Technologies*, 2:1900070, 2019.

[4] Amira Abbas, David Sutter, Christa Zoufal, Aurélien Lucchi, Alessio Figalli, and Stefan Woerner. The Power of Quantum Neural Networks. *Nature Computational Science*, 1:403–409, 2021.

[5] Yuguo Shao, Zhengyu Chen, Zhaohui Wei, and Zhengwei Liu. Diagnosing Quantum Circuits: Noise Robustness, Trainability, and Expressibility, 2025. Available at <https://arxiv.org/abs/2509.11307>.

[6] Evan Greensmith, Peter L. Bartlett, and Jonathan Baxter. Variance reduction techniques for gradient estimates in reinforcement learning. *Journal of Machine Learning Research*, 5:1471–1530, 2004.

[7] Yan Duan, Xi Chen, Rein Houthooft, John Schulman, and Pieter Abbeel. Benchmarking deep reinforcement learning for continuous control. In *International Conference on Machine Learning (ICML)*, pages 1329–1338. PMLR, 2016.

[8] Namjoon Suh and Guang Cheng. A Survey on Statistical Theory of Deep Learning: Approximation, Training Dynamics, and Generative Models, 2024. Available at <https://arxiv.org/abs/2401.07187>.

[9] Namjoon Suh, Tian-Ti Zhou, and Xiaoming Huo. Approximation and non-parametric estimation of functions over high-dimensional spheres via deep relu networks. In *International Conference on Learning Representations (ICLR)*, 2022.

[10] Mikhail Belkin, Daniel Hsu, Siyuan Ma, and Soumik Mandal. Reconciling modern machine-learning practice and the classical bias-variance tradeoff. *Proceedings of the National Academy of Sciences*, 116(32):15849–15854, 2019.

[11] Maithra Raghu, Ben Poole, Jon Kleinberg, Surya Ganguli, and Jascha Sohl-Dickstein. On the expressive power of deep neural networks. In *International Conference on Machine Learning (ICML)*, pages 2847–2854. PMLR, 2017.

[12] Gege Zhang, Gangwei Li, Weining Shen, and Weidong Zhang. The expressivity and training of deep neural networks: Toward the edge of chaos? *Neurocomputing*, 386:8–17, 2020.

[13] Ian Goodfellow, Yoshua Bengio, and Aaron Courville. *Deep Learning*. MIT Press, 2016. <http://www.deeplearningbook.org>.

[14] Razvan Pascanu, Tomas Mikolov, and Yoshua Bengio. On the difficulty of training recurrent neural networks. In *International Conference on Machine Learning (ICML)*, pages 1310–1318. PMLR, 2013.

[15] Diederik P. Kingma and Jimmy Ba. Adam: A Method for Stochastic Optimization. In *International Conference on Learning Representations (ICLR)*, 2015.

[16] Jarrod R. McClean, Sergio Boixo, Vadim N. Smelyanskiy, Ryan Babbush, and Hartmut Neven. Barren plateaus in quantum neural network training landscapes. *Nature Communications*, 9:4812, 2018.

[17] Richard S. Sutton and Andrew G. Barto. *Reinforcement Learning: An Introduction*. MIT press, second edition, 2018.

[18] Greg Brockman, Vicki Cheung, Ludwig Pettersson, Jonas Schneider, John Schulman, Jie Tang, and Wojciech Zaremba. OpenAI Gym, 2016. Available at <https://arxiv.org/abs/1606.01540>.

[19] Rishabh Agarwal, Chen Liang, Dale Schuurmans, and Mohammad Norouzi. Learning to Generalize from Sparse and Under-specified Rewards. In *International Conference on Machine Learning (ICML)*, pages 130–140. PMLR, 2019.

[20] Pranav Saligram, Tanvir Bhathal, and Robby Manhani. 2048: Reinforcement Learning in a Delayed Reward Environment, 2025. Available at <https://arxiv.org/html/2507.05465v1>.

[21] Beining Han, Zhizhou Ren, Zuofan Wu, Yuan Zhou, and Jian Peng. Off-Policy Reinforcement Learning with Delayed Rewards. In *International Conference on Machine Learning (ICML)*, pages 8280–8303. PMLR, 2022.

[22] Octavio Pappalardo, Rodrigo Ramele, and Juan Miguel Santos. Black box meta-learning intrinsic rewards for sparse-reward environments, 2024. Available at <https://arxiv.org/abs/2407.21546>.

[23] Myeongjin Shin, Junseo Lee, and Kabgyun Jeong. Estimating quantum neural information through a quantum neural network. *Quantum Information Processing*, 23:57, 2024.

[24] Donghwa Ji, Junseo Lee, Myeongjin Shin, Ilkwon Sohn, and Kabgyun Jeong. Bounding quantum uncommon information with quantum neural estimators. *Quantum Science and Technology*, 11:015001, 2026.

Appendix

Appendix A: Proof of the Trainability Theorems

First, we prove the Theorem 1. The following relation trivially holds, considering the definitions :

$$g_s(\theta) := \nabla_\theta \eta_s(\theta) = \sum_{a \in A} (\nabla_\theta \pi_\theta(a)) R(a) \quad (\text{A1})$$

$$= \sum_{a \in A} (\nabla_\theta \log \pi_\theta(a)) \pi_\theta(a) R(a) \quad (\text{A2})$$

$$= \mathbb{E}_{a \sim \pi_\theta} [S_\theta(a) R(a)]. \quad (\text{A3})$$

Yet, since

$$\sum_{a \in A} \pi_\theta(a) = 1, \quad (\text{A4})$$

$$\sum_{a \in A} \nabla_\theta \pi_\theta(a) = 0, \quad (\text{A5})$$

$$\equiv \sum_{a \in A} (\nabla_\theta \log \pi_\theta(a)) \pi_\theta(a) = 0, \quad (\text{A6})$$

$$\equiv \mathbb{E}_{a \sim \pi_\theta} [S_\theta(a)] = 0, \quad (\text{A7})$$

then

$$g_s(\theta) = \mathbb{E}_{a \sim \pi_\theta} [S_\theta(a) R(a)] \quad (\text{A8})$$

$$= \mathbb{E}_{a \sim \pi_\theta} [S_\theta(a) R(a)] - \mathbb{E} [S_\theta(a)] \mathbb{E} [R(a)] \quad (\text{A9})$$

$$= \text{Cov}(S_\theta(A), R(A)). \quad (\text{A10})$$

Next, fix an arbitrary unit vector $u \in \mathbb{R}^d$ and define functions f and g as

$$f(a) := \langle u, S_\theta(a) \rangle, \quad g(r) := r. \quad (\text{A11})$$

Our claim is that

Lemma 1. *With the same setting above,*

$$\langle u, g_s(\theta) \rangle = \text{Cov}(f(A), g(R)). \quad (\text{A12})$$

Proof. We already know that for an arbitrary probabilistic vector $X \in \mathbb{R}^d$,

$$\langle u, \mathbb{E} [X] \rangle = \mathbb{E} [\langle u, X \rangle]. \quad (\text{A13})$$

This is simply because

$$(RHS) = \mathbb{E} \left[\sum_{i=1}^d u_i X_i \right] = \sum_{i=1}^d u_i \mathbb{E} [X_i] \quad (\text{A14})$$

$$= \langle u, \mathbb{E} [X] \rangle = (LHS). \quad (\text{A15})$$

Meanwhile,

$$\langle u, \text{Cov}(S_\theta, R) \rangle = \langle u, \mathbb{E} [S_\theta R] - \mathbb{E} [S_\theta] \mathbb{E} [R] \rangle \quad (\text{A16})$$

$$= \langle u, \mathbb{E} [S_\theta R] \rangle - \langle u, \mathbb{E} [S_\theta] \mathbb{E} [R] \rangle. \quad (\text{A17})$$

Applying the results shown above, we get

$$\langle u, g_s(\theta) \rangle = \mathbb{E} [\langle u, S_\theta R \rangle] - \langle u, \mathbb{E} [S_\theta] \mathbb{E} [R] \rangle \quad (\text{A18})$$

$$= \mathbb{E} [\langle u, S_\theta R \rangle] - \mathbb{E} [R] \langle u, \mathbb{E} [S_\theta] \rangle \quad (\text{A19})$$

$$= \mathbb{E} [R \langle u, S_\theta \rangle] - \mathbb{E} [R] \mathbb{E} [\langle u, S_\theta \rangle] \quad (\text{A20})$$

$$= \text{Cov}(\langle u, S_\theta \rangle, R) = \text{Cov}(f(A), g(R)). \quad (\text{A21})$$

□

Also, we already know that

$$|f(a)| \leq \|u\| \|S_\theta(a)\| \leq G_{\max}, \quad |g(r)| \leq R_{\max}, \quad (\text{A22})$$

where the first inequality is trivial due to the Cauchy-Schwarz inequality. Thus, $\|f\|_\infty \leq G_{\max}$ and $\|g\|_\infty \leq R_{\max}$ definitely hold, where $\|f\|_\infty := \sup_t |f(t)|$.

Then

$$\begin{aligned} & \text{Cov}(f(A), g(R)) \\ &= \mathbb{E} [f(A)g(R)] - \mathbb{E} [f(A)] \mathbb{E} [g(R)] \end{aligned} \quad (\text{A23})$$

$$= \sum_a \int_{\mathbb{R}} f(a)g(r) \{p(a, r) - p_A(a)p_R(r)\} dr \quad (\text{A24})$$

$$= \sum_a \int_{\mathbb{R}} f(a)g(r) \{p(a, r) - q(a, r)\} dr \quad (\text{A25})$$

$$= \mathbb{E}_p [fg] - \mathbb{E}_q [fg], \quad (\text{A26})$$

where we use some notations

$$\bullet p_A(a) = \text{Pr}(A = a).$$

$$\bullet p(a, r) = p_A(a)p(r|a) \text{ (joint distribution).}$$

$$\bullet p_R(r) = \sum_a p_A(a)p(r|a).$$

$$\bullet q(a, r) = p_A(a)p_R(r) \text{ (simple, product distribution).}$$

The second inequality holds since

$$\begin{aligned} & \mathbb{E} [f(A)] \mathbb{E} [g(R)] \\ &= \left(\sum_a f(a)p_A(a) \right) \left(\int_{\mathbb{R}} g(r)p_R(r) dr \right) \end{aligned} \quad (\text{A27})$$

$$= \sum_a \int_{\mathbb{R}} f(a)g(r)p_A(a)p_R(r). \quad (\text{A28})$$

Considering the Lemma 1, if we denote $h(a, r) := f(a)g(r)$, we get

$$|\langle u, g_s(\theta) \rangle| = |\mathbb{E}_p [h] - \mathbb{E}_q [h]|. \quad (\text{A29})$$

Now let us introduce the concept of total variation distance (TVD), which is one of the statistical distance metrics between two distributions and is defined as follows in our case:

$$TV(p, q) := \frac{1}{2} \sum_a \int_{\mathbb{R}} |p(a, r) - q(a, r)| dr. \quad (\text{A30})$$

Then

$$|\mathbb{E}_p[h] - \mathbb{E}_q[h]| = \left| \sum_a \int_{\mathbb{R}} h(a, r) \{p(a, r) - q(a, r)\} dr \right| \quad (\text{A31})$$

$$\leq \sum_a \int_{\mathbb{R}} |h(a, r)| |p(a, r) - q(a, r)| dr \quad (\text{A32})$$

$$\leq \|h\|_{\infty} \sum_a \int_{\mathbb{R}} |p - q| dr = 2\|h\|_{\infty} TV(p, q). \quad (\text{A33})$$

The existence of a value $\|h\|_{\infty}$ is automatically proven by

$$\|h\|_{\infty} \leq \|f\|_{\infty} \|g\|_{\infty} \leq G_{\max} R_{\max}. \quad (\text{A34})$$

Hence,

$$|\langle u, g_s(\theta) \rangle| \leq 2G_{\max} R_{\max} TV(p, q) \quad (\text{A35})$$

while according to the Pinsker Inequality

$$TV(p, q) \leq \sqrt{\frac{1}{2} D_{KL}(p||q)}. \quad (\text{A36})$$

Therefore,

$$|\langle u, g_s(\theta) \rangle| \leq 2G_{\max} R_{\max} TV(p, q) \quad (\text{A37})$$

$$\leq 2G_{\max} R_{\max} \sqrt{\frac{1}{2} I(A; Y)} \quad (\text{A38})$$

$$= \sqrt{2} G_{\max} R_{\max} \sqrt{I(A; Y)}. \quad (\text{A39})$$

We also know the trivial fact that

$$\|v\| = \sup_{\|u\|=1} |\langle u, v \rangle| \quad (\text{A40})$$

for an arbitrary vector v . Hence, finally

$$\begin{aligned} \|g_s(\theta)\| &= \sup_{\|u\|=1} |\langle u, g_s(\theta) \rangle| \\ &\leq \sqrt{2} G_{\max} R_{\max} \sqrt{I(A; Y)}. \end{aligned}$$

In big-O style notation,

$$\|g_s(\theta)\| \leq O(\sqrt{I(A; Y)}). \quad (\text{A41})$$

Thus, the Theorem 1 is proved.

Secondly, we prove the Theorem 2. Considering the definitions of \tilde{R} , g , and Δ , it is trivial that

$$R \in B_k \Rightarrow |R - m_k| \leq \frac{\Delta}{2}. \quad (\text{A42})$$

Thus,

$$|R - g(\tilde{R})| \leq \frac{\Delta}{2} \mathbb{E} [|R - g(\tilde{R})|] \leq \frac{\Delta}{2} \quad (\text{A43})$$

hold all the time. We already know that $g_s(\theta) = \text{Cov}(S_{\theta}(A), R)$. Let us decompose R into $R = g(\tilde{R}) + (R - g(\tilde{R}))$ and substitute this to the definition of $g_s(\theta)$ as

$$g_s(\theta) = \text{Cov} \left(S_{\theta}, g(\tilde{R}) + (R - g(\tilde{R})) \right) \quad (\text{A44})$$

$$= \text{Cov} \left(S_{\theta}, g(\tilde{R}) \right) + \text{Cov} \left(S_{\theta}, R - g(\tilde{R}) \right). \quad (\text{A45})$$

Thus,

$$|\|g_s(\theta)\|| \leq \|\text{Cov}(S_{\theta}, g(\tilde{R}))\| + \|\text{Cov}(S_{\theta}, R - g(\tilde{R}))\|. \quad (\text{A46})$$

For $\|\text{Cov}(S_{\theta}, g(\tilde{R}))\|$, fix one of the arbitrary unit vectors $u \in \mathbb{R}^d$ and define the functions f and g' as

$$f(a) := \langle u, S_{\theta}(a) \rangle, \quad g'(k) := g(k) = m_k. \quad (\text{A47})$$

It is trivial that

$$|f| \leq G_{\max}, \quad |g'| \leq R_{\max}. \quad (\text{A48})$$

Hence, with the same logic as Theorem 1,

$$|\langle u, \text{Cov}(S_{\theta}, g(\tilde{R})) \rangle| \leq \sqrt{2} G_{\max} R_{\max} \sqrt{I(A; \tilde{R})} \quad (\text{A49})$$

$$\Rightarrow \|\text{Cov}(S_{\theta}, g(\tilde{R}))\| \leq \sqrt{2} G_{\max} R_{\max} \sqrt{I(A; \tilde{R})}. \quad (\text{A50})$$

For $\|\text{Cov}(S_{\theta}, R - g(\tilde{R}))\|$, Recall the concept of essential supremum, where Y signifies a random variable:

$$\text{ess sup } Y := \inf \{M \in \mathbb{R} : P(Y > M) = 0\} \quad (\text{A51})$$

and introduce a notation $\|X\|_{\infty} := \text{ess sup } \|X\|$. Then the following lemma holds:

Lemma 2. If $\|X\|_{\infty} < \infty$, then $\|\text{Cov}(X, Z)\| \leq 2\|X\|_{\infty} \mathbb{E} [|Z|]$.

Proof. Note that

$$\|\text{Cov}(X, Z)\| = \|\mathbb{E}[XZ] - \mathbb{E}[X]\mathbb{E}[Z]\| \quad (\text{A52})$$

$$\leq \|\mathbb{E}[XZ]\| + \|\mathbb{E}[X]\| \cdot \|\mathbb{E}[Z]\|. \quad (\text{A53})$$

We also know that

$$|\mathbb{E}[V]| \leq \mathbb{E}[|V|], \quad |\mathbb{E}[W]| \leq \mathbb{E}[|W|] \quad (\text{A54})$$

which is trivial, thinking of Jensen's inequality. Therefore,

$$\|\text{Cov}(X, Z)\| \leq \|\mathbb{E}[XZ]\| + \|\mathbb{E}[X]\| \cdot \|\mathbb{E}[Z]\| \quad (\text{A55})$$

$$\leq \mathbb{E}[|X||Z|] + \mathbb{E}[|X|] \cdot \mathbb{E}[|Z|] \quad (\text{A56})$$

$$\leq 2\|X\|_{\infty} \mathbb{E}[|Z|], \quad (\text{A57})$$

where the last inequality follows from $\|X\| \leq \|X\|_{\infty}$. \square

Apply the Lemma 2 to

$$X = S_{\theta}(A), \quad Z = R - g(\tilde{R}). \quad (\text{A58})$$

Then we get

$$\|\text{Cov}(S_{\theta}(A), R - g(\tilde{R}))\| \leq 2 \cdot G_{\max} \cdot \frac{\Delta}{2} = G_{\max} \Delta. \quad (\text{A59})$$

According to both results above, we can get the final inequality

$$\|g_s(\theta)\| \leq \sqrt{2}G_{\max}R_{\max}\sqrt{I(A; \tilde{R})} + G_{\max}\Delta. \quad (\text{A60})$$

This completes the proof of Theorem 2.

Finally, we prove the Theorem 3. First, fix a state s and let us introduce some concepts for the proof;

$$\begin{aligned} g_s(\theta) &:= \nabla_{\theta} \mathbb{E}_{A \sim \pi_{\theta}(\cdot|s)} [Y(s, A)] \\ &= \mathbb{E}_{A \sim \pi_{\theta}(\cdot|s)} [S_{\theta}(s, A)Y(s, A)]. \end{aligned}$$

Again,

$$\mathbb{E}[S_{\theta}(s, A)] = \sum_a \pi_{\theta}(a|s) \nabla_{\theta} \log \pi_{\theta}(a|s) \quad (\text{A61})$$

$$= \sum_a \nabla_{\theta} \pi_{\theta}(a|s) \quad (\text{A62})$$

$$= \nabla_{\theta} \sum_a \pi_{\theta}(a|s) = 0. \quad (\text{A63})$$

Also think of $B(s)$, which denotes an arbitrary function only depends on the state s , as *baseline*. Then

$$\mathbb{E}[S_{\theta}(s, A)B(s)] = B(s)\mathbb{E}[S_{\theta}(s, A)] = 0. \quad (\text{A64})$$

Thus,

$$\mathbb{E}[S_{\theta}(s, A)(Y(s, A) - B(s))] = g_s(\theta) \quad (\text{A65})$$

considering Equation (A63). If we choose $\mathbb{E}[Y|S = s]$ as baseline,

$$\begin{aligned} g_s(\theta) &= \mathbb{E}[S_{\theta}(s, A)Y(s, A)] - \mathbb{E}[S_{\theta}(s, A)B(s)] \\ &= \mathbb{E}[S_{\theta}(s, A)Y(s, A)] - \mathbb{E}[S_{\theta}(s, A) \cdot \mathbb{E}[Y|S = s]] \\ &= \mathbb{E}[S_{\theta}(s, A)Y(s, A)] - \mathbb{E}[S_{\theta}(s, A)]\mathbb{E}[Y|S = s] \\ &= \text{Cov}_{A \sim \pi_{\theta}(\cdot|s)}(S_{\theta}(s, A), Y(s, A)). \end{aligned} \quad (\text{A66})$$

Divide Y into $\tilde{Y} \in \{1, 2, \dots, B\}$ and define m_k as explained above. Then we can define

$$Y_q := g(\tilde{Y}) = m_{\tilde{Y}}. \quad (\text{A67})$$

Using the same decomposition technique shown in the Theorem 2,

$$\text{Cov}(S_{\theta}, Y) = \text{Cov}(S_{\theta}, Y_q) + \text{Cov}(S_{\theta}, Y - Y_q) \quad (\text{A68})$$

and

$$\begin{aligned} \|\text{Cov}(S_{\theta}, Y)\| &\leq \|\text{Cov}(S_{\theta}, Y_q)\| + \|\text{Cov}(S_{\theta}, Y - Y_q)\| \\ &\quad (\text{A69}) \end{aligned}$$

$$\leq \sqrt{2}G_{\max}Y_{\max}\sqrt{I(A; \tilde{Y}|S = s)} + G_{\max}\Delta. \quad (\text{A70})$$

Thus,

$$\|g_s(\theta)\| \leq \sqrt{2}G_{\max}Y_{\max}\sqrt{I(A; \tilde{Y}|S = s)} + G_{\max}\Delta. \quad (\text{A71})$$

Then it suffices to show the following lemma:

Lemma 3.

$$\nabla_{\theta}\eta'(\theta) = \mathbb{E}_{s \sim d_{\pi}} [g_s(\theta)], \quad (\text{A72})$$

where

$$\rho_{\pi}(s) := \sum_{t=0}^{T-1} \gamma^t \Pr(s_t = s), \quad d_{\pi}(s) := \frac{1-\gamma}{1-\gamma^T} \rho_{\pi}(s) \quad (\text{A73})$$

Proof. Take the derivatives of η' .

$$\nabla_{\theta}\eta'(\theta) = \frac{1-\gamma}{1-\gamma^T} \sum_{t=0}^{T-1} \mathbb{E}[\nabla_{\theta} \log \pi_{\theta}(a_t|s_t) \cdot G_t] \quad (\text{A74})$$

$$= \frac{1-\gamma}{1-\gamma^T} \sum_{t=0}^{T-1} \mathbb{E}[S_{\theta}(s_t, a_t) \cdot G_t]. \quad (\text{A75})$$

Note that

$$\begin{aligned} \mathbb{E}[G_t|s_t, a_t] &= \gamma^t \mathbb{E}\left[\sum_{m=0}^{T-t-1} \gamma^m R_{t+m} \mid s_t, a_t\right] \\ &= \gamma^t Q^{\pi_{\theta}}(s_t, a_t). \end{aligned}$$

Thus,

$$\nabla_{\theta}\eta'(\theta) = \frac{1-\gamma}{1-\gamma^T} \sum_{t=0}^{T-1} \gamma^t \mathbb{E}[S_{\theta}(s_t, a_t) \cdot Q^{\pi_{\theta}}(s_t, a_t)]. \quad (\text{A76})$$

For arbitrary $\phi(s, a)$,

$$\frac{1-\gamma}{1-\gamma^T} \sum_{t=0}^{T-1} \gamma^t \mathbb{E}[\phi(s_t, a_t)] \quad (\text{A77})$$

$$= \frac{1-\gamma}{1-\gamma^T} \sum_{t=0}^{T-1} \gamma^t \sum_{s, a} \Pr(s, a) \phi(s, a) \quad (\text{A78})$$

$$= \sum_{s, a} \left(\frac{1-\gamma}{1-\gamma^T} \sum_{t=0}^{T-1} \gamma^t \Pr(s) \right) \pi_{\theta}(a|s) \phi(s, a) \quad (\text{A79})$$

$$= \sum_s d_{\pi}(s) \sum_a \pi_{\theta}(a|s) \phi(s, a) \quad (\text{A80})$$

$$= \mathbb{E}_{S \sim d_{\pi}, A \sim \pi_{\theta}} [\phi(S, A)]. \quad (\text{A81})$$

Substitute $\phi(s, a) = S_{\theta}(s, a)Q^{\pi_{\theta}}(s, a)$, then

$$\nabla_{\theta}\eta'(\theta) = \mathbb{E}_{S \sim d_{\pi}, A \sim \pi_{\theta}} [S_{\theta}(S, A)Q^{\pi_{\theta}}(S, A)] \quad (\text{A82})$$

$$= \mathbb{E}_{S \sim d_{\pi}} [\mathbb{E}_{A \sim \pi_{\theta}(\cdot|s)} [S_{\theta}(s, A)Q^{\pi_{\theta}}(s, A)]] \quad (\text{A83})$$

$$= \mathbb{E}_{S \sim d_{\pi}} [g_s(\theta)]. \quad (\text{A84})$$

□

Therefore,

$$\|\nabla_\theta \eta'(\theta)\| = \|\mathbb{E}_{S \sim d_\pi} [g_s(\theta)]\| \quad (\text{A85})$$

$$\leq E_{S \sim d_\pi} [|g_s(\theta)|] \quad (\text{A86})$$

$$\leq \mathbb{E}_{S \sim d_\pi} \left[\sqrt{2G_{\max} Y_{\max} \sqrt{I(A; \tilde{Y}|S=s)} + G_{\max} \Delta} \right] \quad (\text{A87})$$

$$\leq \sqrt{2G_{\max} Y_{\max}} \sqrt{\mathbb{E}_{S \sim d_\pi} [I(A; \tilde{Y}|s=s)]} + G_{\max} \Delta. \quad (\text{A88})$$

The first and last inequality hold due to the Jensen's inequality, again. This proves Theorem 3.

Appendix B: Proof of the Expressivity Theorem

Take expectations to the both sides of Equation (45). Then we get

$$\mathbb{E}_{S \sim d_\pi} [JSD_{w(s)}(\{w_i^s\})] = \mathbb{E}_{S \sim d_\pi} [I(A; Z|S=s)] \quad (\text{B1})$$

$$= I(A; Z|S). \quad (\text{B2})$$

Again, fix a state s and

$$I(A; Z, \tilde{Y}|S=s) \quad (\text{B3})$$

$$= I(A; \tilde{Y}|S=s) + I(A; Z|\tilde{Y}|S=s) \quad (\text{B4})$$

$$= I(A; Z|S=s) + I(A; \tilde{Y}|Z, S=s). \quad (\text{B5})$$

With the given assumption,

$$I(A; \tilde{Y}|S=s) = I(A; Z|S=s) + I(A; \tilde{Y}|Z, S=s). \quad (\text{B6})$$

Thus,

$$I(A; \tilde{Y}|S=s) \geq I(A; Z|S=s), \quad (\text{B7})$$

$$\mathbb{E}_{S \sim d_\pi} [I(A; \tilde{Y}|S=s)] \geq \mathbb{E}_{S \sim d_\pi} [I(A; Z|S=s)], \quad (\text{B8})$$

$$\equiv I(A; \tilde{Y}|S) \geq I(A; Z|S) \quad (\text{B9})$$

$$= \mathbb{E}_{S \sim d_\pi} [JSD_{w(s)}(\{\pi_i^s\})]. \quad (\text{B10})$$

So, the Theorem 4 holds for JSD.

Now, consider the L2 Divergence. Note that

$$\|\pi_i^s - \bar{\pi}^s\|_2^2 \quad (\text{B11})$$

$$\leq \|\pi_i^s - \bar{\pi}^s\|_1^2 = 4\text{TV}(\pi_i^s, \bar{\pi}^s)^2 \quad (\text{B12})$$

$$\leq 2D_{KL}(\pi_i^s || \bar{\pi}^s) \quad (\text{B13})$$

$$\Rightarrow w_i(s) \|\pi_i^s - \bar{\pi}^s\|_2^2 \leq 2w_i(s) D_{KL}(\pi_i^s || \bar{\pi}^s) \quad (\text{B14})$$

$$\Rightarrow D_2(Z|s) = \sum_i w_i(s) \|\pi_i^s - \bar{\pi}^s\|_2^2 \quad (\text{B15})$$

$$\leq 2 \sum_i w_i(s) D_{KL}(\pi_i^s || \bar{\pi}^s) = 2I(A; Z|S=s). \quad (\text{B16})$$

Take expectations to the both sides, then

$$\mathbb{E}_{S \sim d_\pi} [D_2(Z|S=s)] \leq 2I(A; Z|S) \leq 2I(A; \tilde{Y}|S). \quad (\text{B17})$$

So, the Theorem 4 holds for L2 Divergence.

Now, consider the TV Divergence. Note that

$$TV(\pi_i^s, \bar{\pi}^s)^2 \leq \frac{1}{2} D_{KL}(\pi_i^s || \bar{\pi}^s) \quad (\text{B18})$$

$$D_{TV}(Z|s) = \sum_i w_i(s) TV(\pi_i^s, \bar{\pi}^s)^2 \quad (\text{B19})$$

$$\leq \frac{1}{2} \sum_i w_i(s) D_{KL}(\pi_i^s || \bar{\pi}^s) = \frac{1}{2} I(A; Z|S=s). \quad (\text{B20})$$

Take expectations to the both sides again and

$$\mathbb{E}_{S \sim d_\pi} [D_{TV}(Z|S=s)] \leq \frac{1}{2} I(A; Z|S) \leq \frac{1}{2} I(A; \tilde{Y}|S). \quad (\text{B21})$$

So, the Theorem 4 holds for TV Divergence.

Appendix C: Experimental Results with Bin Count 10

We present here the numerical results obtained using the same experimental setup as before, but with the bin count set to 10. We begin by showing the overall learning curves of those three different PQC settings. Based on the results shown in Figure 6, the configuration with moderate expressivity again demonstrates the best performance in terms of both effective convergence and overall learning stability. In contrast, both the deep and shallow configurations perform noticeably worse than the moderate case in this experiment. The shallow model, as before, undergoes early stopping, indicating its insufficient expressivity. Notably, the deep configuration performs clearly worse than the default moderate configuration in this setting, a difference that stands out more prominently than in the previous experiment. It appears that stochasticity in this run accentuated the performance gap between the two.

Next, we examine the relationship between MI-TET and the policy entropy. As expected, this experiment exhibits trends that are consistent with the earlier results. The fact that this relationship persists even under a different discretization setting further strengthens the validity of the underlying phenomenon. In other words, the consistency across bin counts provides additional evidence that MI-TET reliably captures the *concentration* of the learning process. It is also quantitatively validated if we look at the correlation coefficient between MI-TET and the policy entropy in the Appendix D.

The final set of results concerns the validation of our theorem. Because discretization with a relatively low bin count of 10 removes some informative structure from MI-TET, its magnitude becomes undesirably small. This necessitates estimating and applying an appropriate scaling constant, as we have examined earlier.

The following two figures (Figure 8, Figure 9) present the raw results and the scaled results, respectively.

The intuition in estimating the constant is simple. First, for simplicity, we ignore the discretization error term in the trainability inequality. It is because such a translation has little to do with the actual scale and trend of the real MI-TET graph,

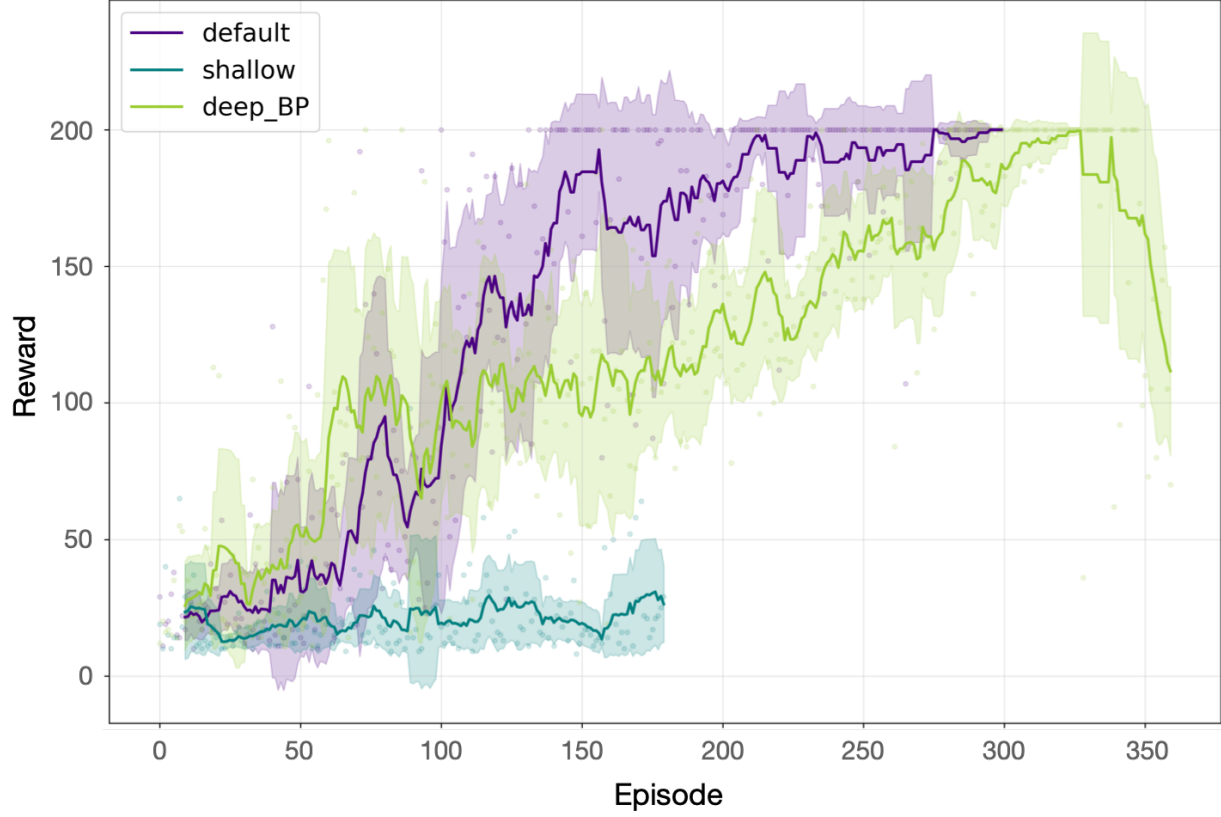


FIG. 6: **Overall learning progress of the total tree cases: *default*, *shallow*, *deep_BP*.** Each colored point represents the actual reward obtained in each batch for a given PQC setting, while the corresponding bold colored line indicates the 10-batch moving average of the reward for that setting.

just moving the total graph upward. Since we already know theoretically that our two inequality are valid, we know that

$$(\text{gradient norm}) \leq C \cdot \sqrt{\text{MI-TET}}, \quad (\text{C1})$$

and

$$(\text{Expressivity}) \leq K \cdot \text{MI-TET}. \quad (\text{C2})$$

Just because we are going to use time-dependent log of those MI-TET, gradient norm, Expressivity, these values would be temporarily changed. Then we now estimate the constant factors C, K as

$$C \approx \sup_t \frac{\text{gradient norm}}{\sqrt{\text{MI-TET}}}, \quad (\text{C3})$$

$$K \approx \sup_t \frac{\text{Expressivity}}{\text{MI-TET}}. \quad (\text{C4})$$

Using this estimation process, we get the constant factor for each setting as follows:

Although we now get the desired upper bound relations as shown in Figure 9, it is still undesirable considering their

‘tightness’ to the actual gradient norm / expressivity values: in pursuing the desired inequality relationship, we inevitably lose another important property—tightness. The fundamental reason for this issue is that the scale of MI-TET does not naturally align with the scales of the gradient norm or expressivity. Therefore, in one sentence, ‘*bin count still matters*.’

	Shallow	Default	Deep
C	1.2158	7.5646	9.3546
K	6.1212	2.8592	5.9357

TABLE I: **Constant factors for each process.**

Appendix D: Correlation Matrices

Please look at Figure 10 in the following.

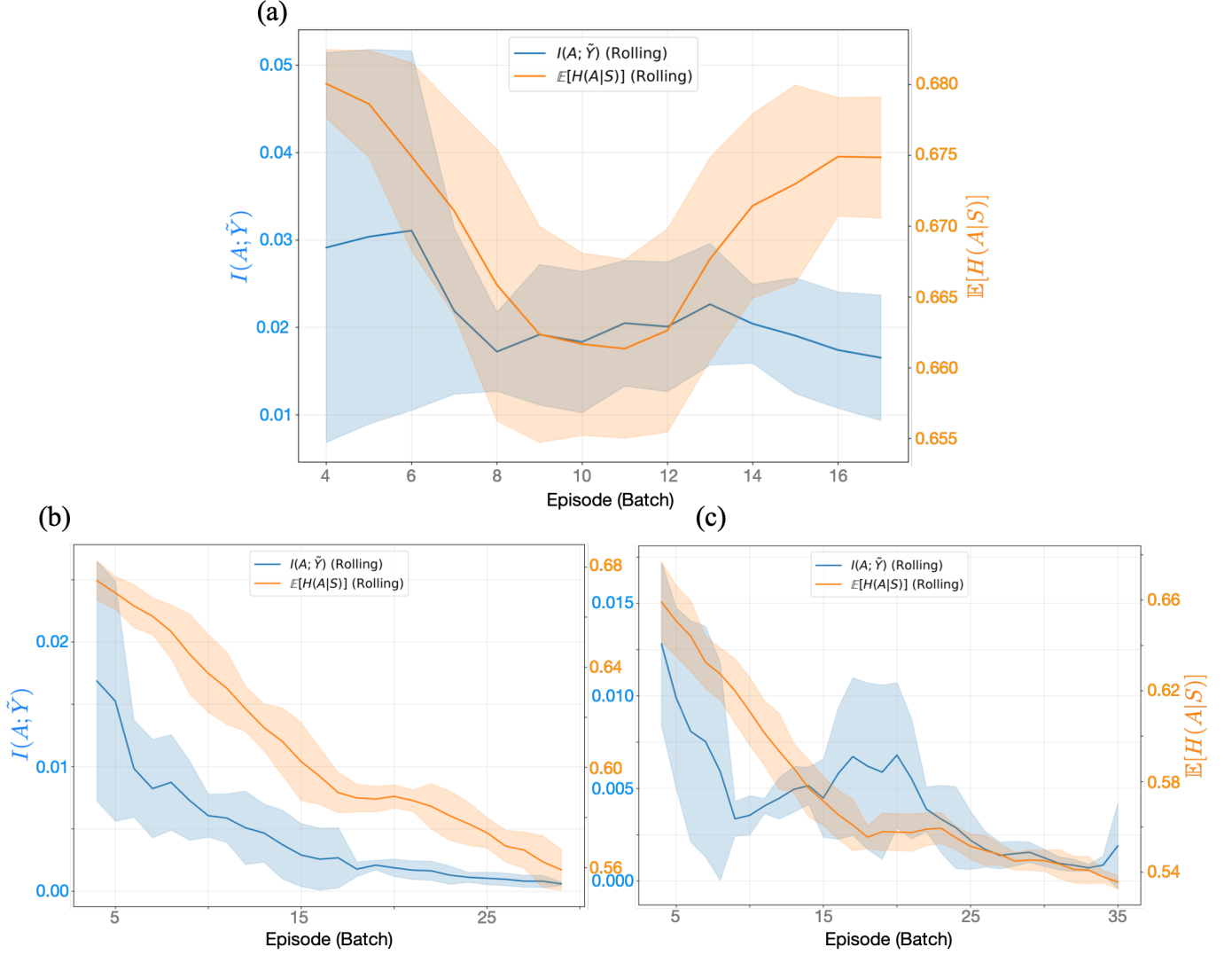


FIG. 7: Comparison of MI-TET trends for the three configurations with the policy entropy $H(A|S)$: (a) Shallow, (b) Default, and (c) Deep_BP.

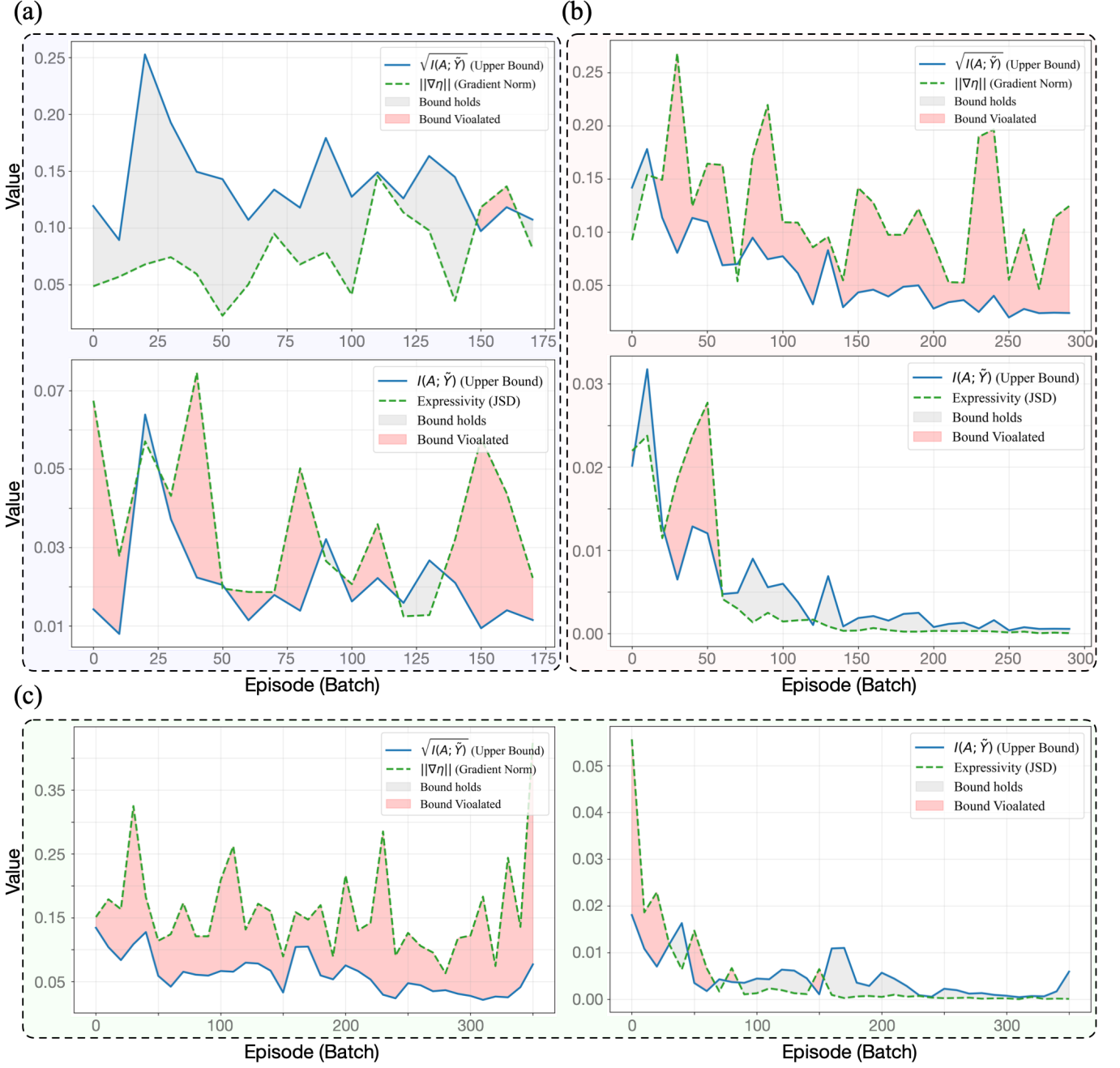


FIG. 8: **Theorem validation with the different PQC structure.** Note that these are literally ‘raw’ data, without any scaling factor is multiplied to both $I(A; \tilde{Y})$ and $\sqrt{I(A; \tilde{Y})}$: (a) Shallow, (b) Default, and (c) Deep_BP.

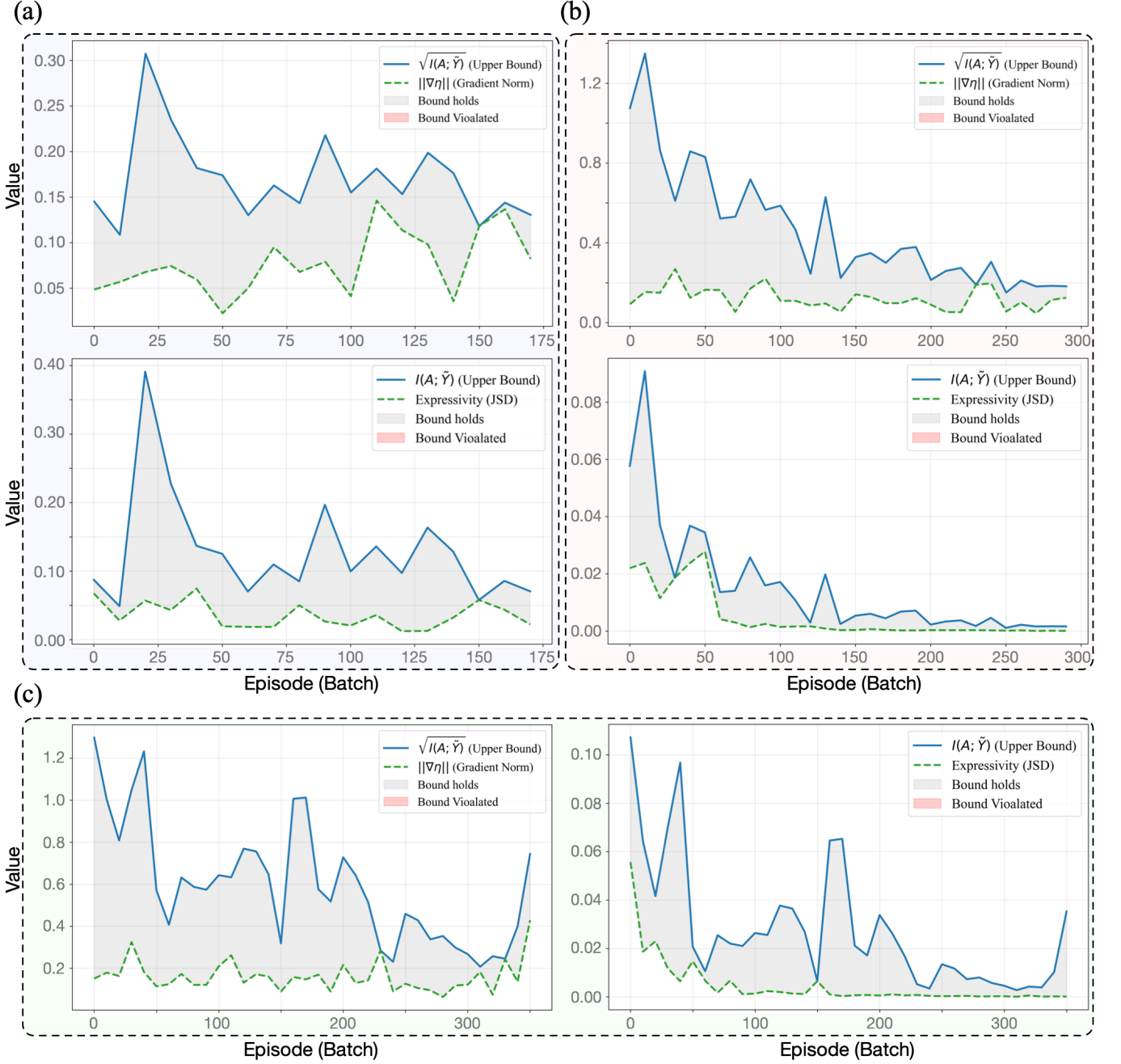


FIG. 9: **Theorem validation with the different PQC structure.** Remark that it is the result of applying some constant factor C and K to $I(A; \tilde{Y})$ and $\sqrt{I(A; \tilde{Y})}$, respectively. The constant factor was estimated using the given motivation in the paragraph: (a) Shallow, (b) Default, and (c) Deep_BP.

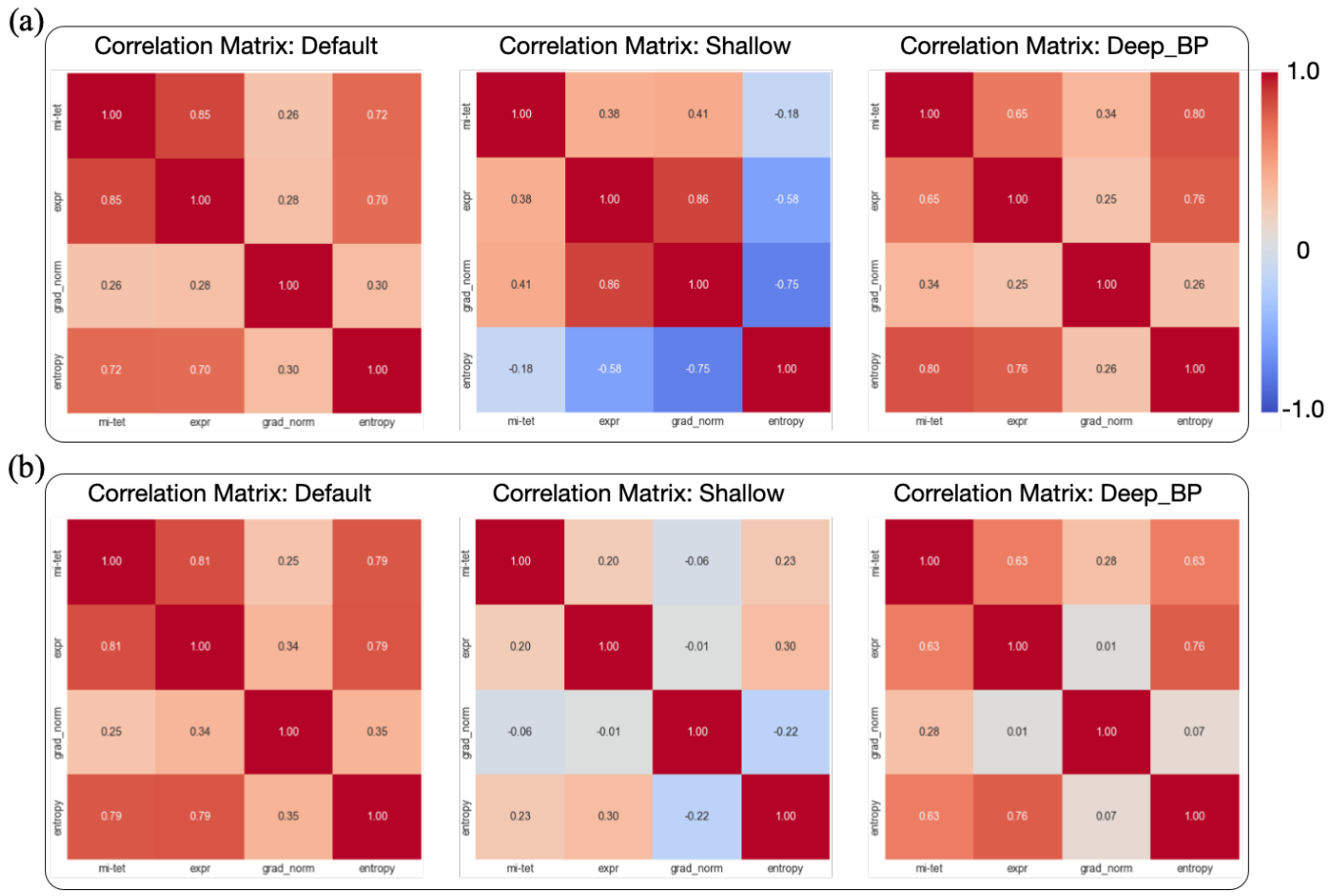


FIG. 10: Correlation matrices for both bin count of 50 (a) and 10 (b).